AD-A037 143 NORTHROP CORP ANAHEIM CALIF ELECTRO-MECHANICAL DIV F/G 17/5
EXPERIMENTAL DEVELOPMENT OF A FLIR SENSOR PROCESSOR.(U)
NOV 76 T NODA, H HENNING, T LEIBOFF DAAG53-76-C-0188
UNCLASSIFIED NORT-76Y133A NL

OF
AD
A037143

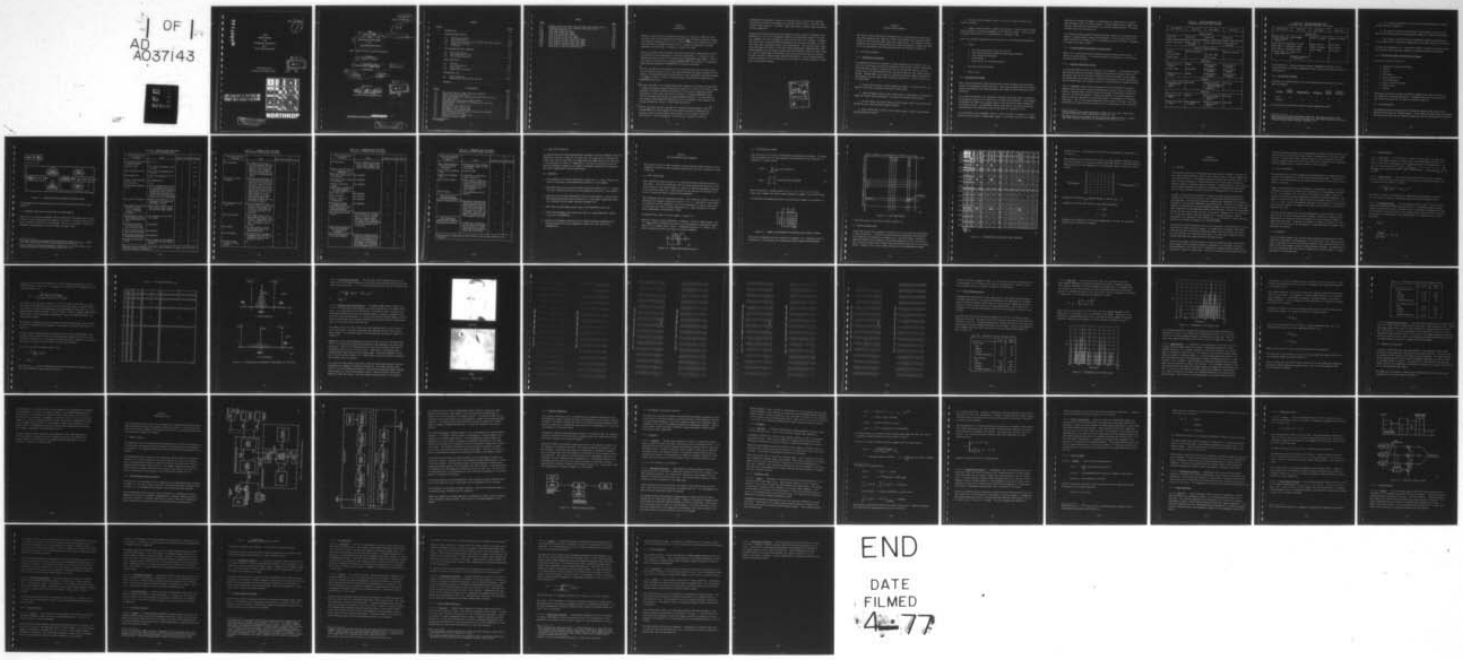

END

DATE
FILMED
4-77

Report No. 76Y133A

FIRST
QUARTER REPORT
FOR
EXPERIMENTAL DEVELOPMENT
OF A
FLIR SENSOR PROCESSOR

30 September 1976
(Revised 30 November 1976)

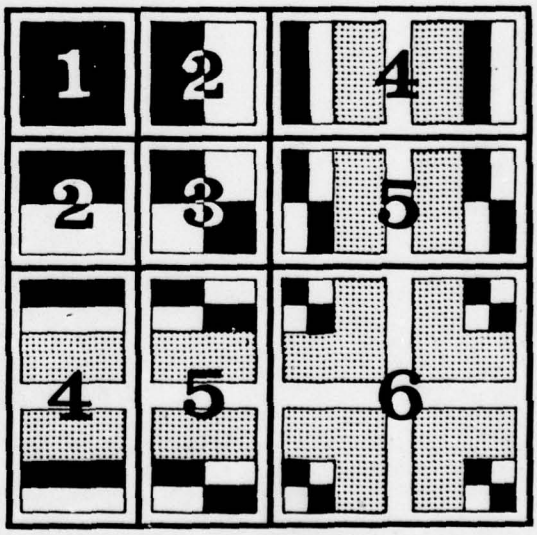

NORTHROP

(14) NORTL

Report No. 76Y133A

(1)

(9) FIRST QUARTER REPORT no. 1, 1 Jul-30 Sep 76,

FOR

(6) EXPERIMENTAL DEVELOPMENT
OF A
FLIR SENSOR PROCESSOR

(Not complete without classified Appendix)

(15) Contract
DAAG53-76-C-0188

(11) 30 September 1976
(Revised 30 November 1976)

(12) 62p.

Prepared by

(10) T. Noda,
H. Henning,
T. Leiboff,
G. Robinson
T. Baxter
B. Deal

Approved by

Ross Chiles, Manager
Automation Systems Engineering

388 834

Northrop Corporation Electro-Mechanical Division
500 East Orangethorpe Avenue, Anaheim, California 92801

NORTHROP

CONTENTS

ILLUSTRATIONS

*See Addendum

TABLES

SECTION 1
INTRODUCTION

Northrop Corporation, Electro-Mechanical Division, is pleased to submit the first quarterly report of the Experimental Development of a FLIR Sensor Processor program. The program's funding started on July 1, 1976, and this report summarizes the technical performance through September 30, 1976, marking the completion of Task 1, Experiment and Study Plan, of Contract No. DAAG53-76-C-0188.

Section 2 contains a brief Advanced Scout Helicopter mission scenario used to bound the problem of a FLIR operating in a difficult environment. It includes a table showing the effect of some of the operational parameters on image quality. Parts of this section, which have been classified SECRET, have been included in a separately bound appendix along with a bibliography of background documents.

Section 3 provides a basic definition of the Haar functions, since the Haar transform provides the basis for all of the image processing techniques presented in this report. The Rationalized Haar functions used in these experiments are also discussed in Patent No. 3981443, "Class of Transform Digital Processors for Compression of Multi-Dimensional Data."

Section 4 describes a set of image descriptors designed to facilitate the evaluation of images and image processing algorithms throughout the course of this study. Using groupings of the Haar transform coefficients, a vector whose components are the descriptors of Tone, Edge, and Texture is defined. Computer simulations using stored photographs were utilized to develop these descriptors. The next phase of this program, where controlled experiments will be performed on test imagery, will further evaluate the utility of these image descriptors.

Section 5 includes the basic approach for conducting the experiments, Tasks II through VI of the contract. This section briefly describes the Northrop two-dimension sensor processor, video test equipment and the computer simulation test setups. It then proceeds with the objectives, conceptual solutions,

and generalized experimental approach to principal areas in which Haar transform processing can improve FLIR imaging and operating characteristics. Specific areas covered include autofocus, autodeblur, image enhancement, adaptive signal processing and data compression.

During this reporting period, the two-dimensional sensor processor developed during Northrop's CY 75 and CY 76 Independent Research and Development program, video and test equipment (as shown in Figure 5-1 which follows) have been completed. Programs have been written to interface the minicomputer with the sensor processor, the magnetic tape unit, high-speed printer, and teletypewriter. This has also been a learning period where the effects of the many hardware-implemented image processing algorithms designed into the sensor processor have been observed, using live video inputs. As a result, several minor modifications have been incorporated into the processor and test fixtures to improve their operating capabilities. We are looking forward to the next quarter of this program when we will begin to perform quantitative experiments on controlled imagery.

SECTION 2
MISSION/SYSTEMS ANALYSIS

This section briefly describes the Advanced Scout Helicopter mission, and details all system parameters and visionics on board the Advanced Scout Helicopter (ASH)/ Advanced Attack Helicopter (AAH) that affect image quality. The analysis of these parameters and visionic specifications will bound the problem, to assure the validity of the experimental and study approaches that are outlined in Section 5.

2.1 ASH MISSION SCENARIO

2.1.1 ASH/AAH TADS Description

An experimental FLIR sensor processor is being developed in this phase of the contract for an ASH Target Acquisition Designation System (TADS) visionics application. This FLIR sensor processor could also be used in the AAH TADS Visionics System, because there is a good possibility that the ASH and AAH will have common visionics systems. ASH/AAH TADS will be used for acquiring, tracking, ranging, designating and engaging tank-size targets under day/night conditions. It will be used in the following modes:

a. Laser Detection Mode to detect designated targets. The laser tracker will operate in autotrack, autosearch, and manual search modes.

b. Laser Designation Mode to hold a laser beam on a stationary or moving point target for handoff and/or designation for semiactive terminal homing weapons.

c. Gun and Rocket Fire Control Mode to provide target range and pointing information for use in gun and rocket weapons delivery.

d. Sight Cueing Mode to provide line-of-sight cueing by other on-board sighting and navigation systems.

e. Night Low Level Navigation Mode to be used as a night pilotage aid by either crew member.

f. Target Acquisition Mode to enable the operator to visually search for and acquire targets for day/night engagement at the specified ranges. Initial search and target acquisition will be accomplished in a minimum of time.

TADS is an integrally mounted turret and consists of the following subassemblies:

a. Turret:

1. Day Viewing Subsystem (Direct View and TV)
2. Night Viewing Subsystem (FLIR) and FLIR Sensor Processor
3. Laser Rangefinder/Designator
4. Laser Tracker
5. Stabilization and Tracking Subsystem

b. Electronic/Signal Processing

c. Optical Relay.

2.1.2 AAH Operational Modes

One of the AAH operational modes uses the aerial scout helicopter (the AAH remote aerial scout designation operational mode). This report concentrates on the mission scenario pertaining to this AAH operational mode using the ASH as the aerial scout helicopter.

In the AAH remote aerial scout designation (ASH/AAH) operational mode of operation, ASH designates targets for the AAH with an on-board laser designator. ASH continues to designate the target until missile impact, while the AAH can remask immediately after missile launch. The ASH/AAH helicopter survivability and time line analysis associated with this operational mode are discussed in references 1 and 2.

In the autonomous (self-designate) mode the attack helicopter is masked in a firing position until directed to engage enemy targets. The attack helicopter then unmasks,

identifies the target and engages it, designating the target with its on-board laser designator until the missile impacts. AAH may engage several targets from the same firing position before moving to alternate firing positions. The attack continues until directed otherwise.

In the remote ground designation operational mode, targets for the AAH are designated by a ground operator using a laser designator. After missile launch, the attack helicopter can remask, while the designator operator continues to designate the target until missile impact.

2.1.3 A Typical ASH/AAH Operational Procedure Guide

Table 2-1 is a simplified typical ASH/AAH operational mode procedure guide. It depicts one popup position. For multiple popups the procedure for the one popup position would be repeated.

2.1.4 A Typical AAH Mission Profile

A typical AAH mission profile is discussed in the appendix. The discussion includes AAH cruising speeds and altitudes; distance traveled between various preselected positions; times at the positions; hovering and firing altitudes; firing ranges; the maximum AAH speed during search, tracking, and acquisition modes; AAH maneuverability capabilities; and a graphic portrayal of AAH conducting a defensive mission.

Prior to engagement, aerial scout helicopters provide coordination with ground maneuver units and conduct initial reconnaissance to select routes of ingress and egress of holding areas, attack positions, and primary and alternate firing positions for the attack helicopters. During the operation, the scout helicopters acquire, identify, and hand off targets and assist in the movement of the attack helicopters. This is done using appropriate terrain flight techniques. The scout helicopters may lead the attack helicopters from a holding area to the attack and

---

[1] Issues Related to Helicopter Operating in Combat (U), D. L. Hall, October 1975, Northrop Corporation, Electro-Mechanical Division No. 7292

[2] AAH Remote Aerial Scout Designation Mode Operational Analysis (U), T. G. Baxter, July 1976, Northrop Corporation, Electro-Mechanical Division No. 7742

Table 2-1. ASH/AAH OPERATIONAL MODE PROCEDURAL GUIDE (ONE POPUP POSITION)

ASH Observer	ASH Pilot	AAH Gunner	AAH Pilot
Before Arrival			
Check map Check communications Check sight/laser	Check map Check communications Check radio frequencies	Check map Check communications Check sight/seeker	Check map Check communications Check radio frequencies
Arrival at Popup Position			
Sight on Say when ready Say to start	Position aircraft - -	- Say when ready Say to start	Position aircraft - -
ASH Popup			
Require pilot to unmask Locate target Require pilot to remask	Unmask Hold unmask Remask	Hold position (masked) Hold position (masked) Hold position (masked)	Hold position (masked) Hold position (masked) Hold position (masked)
Remasked			
Give handoff information to AAH gunner	Hold mask	Receive and plot target information from ASH aerial observer	Hold mask
ASH Popup			
Require pilot to unmask Search and acquire target	Unmask Hold unmask until countdown	Prepare information and plan for search Prepare information and plan for search	Hold mask Hold mask

Table 2-1. ASH/AAH OPERATIONAL MODE
PROCEDURAL GUIDE (ONE POPUP POSITION) (Continued)

ASH Observer	ASH Pilot	AAH Gunner	AAH Pilot
ASH/AAH Popup			
Request AAH to unmask on command "Laser On"	Hold unmask	Search for target	Unmask on command
Hold sight on target	Turn on laser	Report lock-on	Hold unmask
Hold sight on target	Lase target	Report AAH detect	Hold position
Hold sight on target	Lase target	Launch weapon	Then remask
"Verify smoke" on target handed off	Laser off	-	-
-	Remask after smoke verification	-	-

firing positions. During the attack, specific engagement techniques from the firing positions will differ, depending on which of the three operational modes is being employed.

2.1.5 ASH Aircrew Functions

Following is an identification of the ASH functions and the ASH aircrew to whom they are assigned:

Crewman	Flight Control	Communications	Navigation	System Monitor	Mission Execution
Pilot	X			X	
Observer		X	X		X

The following conclusions were made in a recent government study:[3]

[3]Advanced Scout Helicopter Man-Machine Interface Investigation Aviation Team, Human Engineering Applications Directorate, U.S. Army Human Engineering Laboratory, Aberdeen Proving Ground, Maryland, September 1975

a. The proposed ASH provides the aircrew with excellent day/night standoff target acquisition capability.

b. The analysis indicates that workload is anticipated to be high in day nap of earth (NOE) operation and exceeds crew capability in night NOE operations.

c. The workload could be reduced by considering automation and integration in the flight control, navigation, communication, and target acquisition functions.

The general recommendation is: Specialized research is needed in conducting night NOE operations using electronic displays to ascertain attention requirements.

2.1.6 ASH Mission Segment Functional Block Diagram

ASH mission functions consist of:

a. Premission briefing and planning
b. Takeoff
c. Enroute
d. Observation
e. Direct artillery fire
f. Direct AAH attack
g. Direct tactical airstrike
h. Return to base
i. Landing.

Observation and direct AAH attack ASH mission segments are of most interest for the ASH/AAH TADS visionics application. An example functional block diagram of the observation portion of the mission is shown in Figure 2-1.

2.2 ASH SURVIVABILITY

The appendix discusses the safe level of helicopter exposure times versus range against various Soviet air defense systems. It also indicates where these air defenses are located and what these air defense systems rely upon for acquisition and detection.

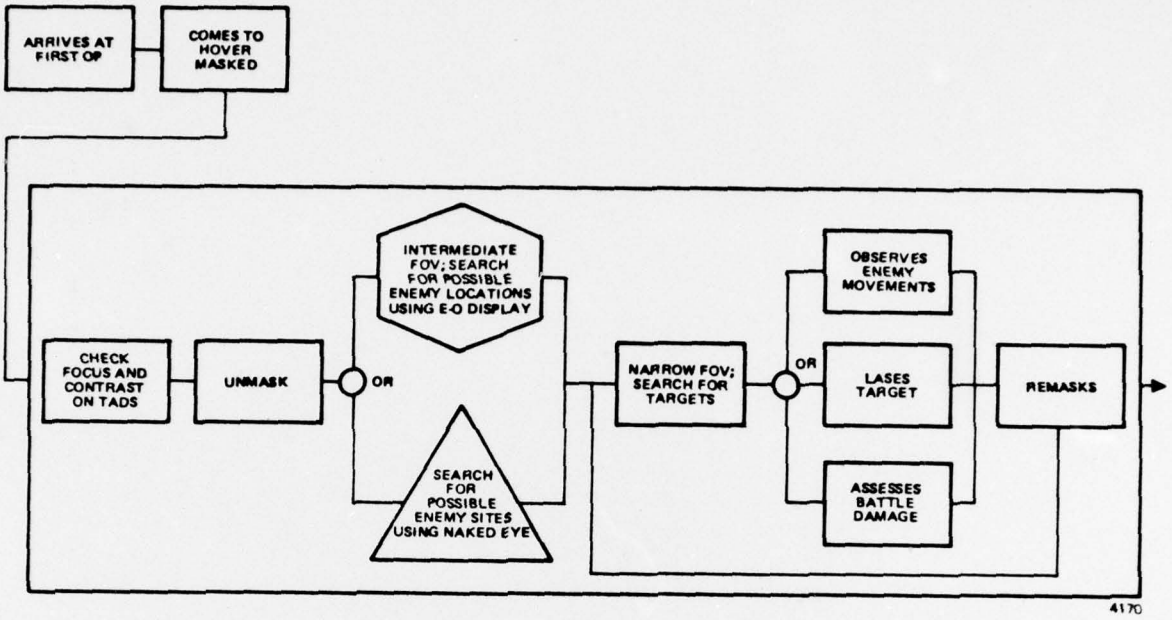

Figure 2-1. OBSERVATION MISSION SEGMENT FLOW BLOCK DIAGRAM

Recommendations are made regarding the flying techniques employed against these threats.[4,5]

2.3 PARAMETERS THAT AFFECT THE ASH TADS FLIR IMAGE QUALITY

Table 2-2 is a listing of parameters that can affect the FLIR image quality of the ASH TADS. This listing gives the parameter, its value, its security classification, and the reference from which it was obtained. The list is intended to bound the parameters being addressed in the FLIR Sensor Processor Study.

---

[4] AAH Remote Aerial Scout Designation Mode Operational Analysis (U), T. G. Baxter, July 1976, Northrop Corporation, Electro-Mechanical Division No. 7742

[5] Issues Related to Helicopter Operating in Combat (U), D. L. Hall, October 1975, Northrop Corporation, Electro-Mechanical Division No. 7292

Table 2-2. PARAMETERS THAT CAN AFFECT ASH TADS FLIR IMAGE QUALITY

TADS FLIR Subsystem Parameter	Value	Classification	Reference
FLIR Spectral Sensitivity Operating Region	8 to 14 μ	U	4,5
FLIR Wide FOV*	≈524 x 698 milliradians (~30° x ~40°)	U	4,5
FLIR Intermediate FOV	175 to 314 milliradians (10° to 18°)	U	4,5
FLIR Narrow FOV	35 to 70 milliradians (2° to 4°)	U	4,5
Nominal FLIR Frame Rate	30 frames/second	U	4,5
FLIR Interlace	2 to 1	U	4,5
Antistreaking Compensation	FLIR has compensation circuitry to eliminate the loss of information encountered when viewing very high contrast targets and to prevent the loss of terrain details when viewed with a sky background	U	5
FLIR Polarity Reversal	Operator selectable and no readjustment of contrast and brightness controls	U	4,5
FLIR Automatic and Semiautomatic control (i.e., brightness, contrast, and gain controls)	Desired where feasible to reduce operator task loading and optimize image quality	U	4,5
FLIR Duration of View - Field Change Switching and Settling Time for View	Field changes are less than 1/2 second	U	4,5
FLIR System Intensity Transfer Curves for Low Contrast Setting	See Appendix	C	5
FLIR SIT Curves for Maximum Contrast Setting	See Appendix	C	5
FLIR Minimum Resolvable Temperature Difference	See Appendix	C	5
FLIR Optical/Electronic Noise	Not be evident on the displays and be less than one shade of gray	U	4,5

*The wide FOV is required to allow the copilot/observer to assist the pilot with enroute checkpoint navigation.

Table 2-2. PARAMETERS THAT CAN AFFECT ASH TADS FLIR IMAGE QUALITY (Continued)

TADS FLIR Subsystem Parameter	Value	Classification	Reference
FLIR Crosstalk	The signal at the output of any nonirradiated detector does not exceed 5% of the signal in the irradiated detector and no signal in any other channel that exceeds 5% of the generating signal.	U	4,5
FLIR Dead and Noisy Channels	Noise Equivalent Temperature Difference (NETD) does not exceed 0.5°C in the center 20% of the sensor FOV and throughout the rest of the FOV the number of inactive channels or channels whose NETD exceeds 0.5°C is not greater than 3% of the total number of channels. Defective channels are separated by more than four acceptable channels.	U	4,5
FLIR Distortion Across Total FOV	Does not exceed 10% of the vertical field in either the vertical or horizontal direction in the center 50% of the FOV and 20% of the remainder.	U	4,5
FLIR Optical Focus	Proper image quality to be maintained (by passive temperature compensation) from 0.5 km to infinity for all FOVs. Automatic focus is desired.	U	5
FLIR Display	FLIR video output to drive the displays required by AMC-SS-AAH-1000A.	U	5
FLIR Performance	The FLIR sensor performance parameters will meet the requirements cited in paragraphs 2.1 and 2.2.	U	4,5
FLIR Aspect Ratio (vertical to horizontal)	3:4	U	4,5

Table 2-2. PARAMETERS THAT CAN AFFECT ASH TADS FLIR IMAGE QUALITY (Continued)

TADS FLIR Subsystem Parameter	Value	Classification	Reference
FLIR Derotation	The FLIR presents the gunner with an erect image at all turret gimbal angles with respect to helicopter axes.	U	5
TADS Acquisition Range Parameter			
TADS Night Target Detection Ranges	See Appendix	C	5,6
TADS Night Target Recogtion Ranges	See Appendix	C	5,6
TADS Day Acquisition Range	See Appendix	C	5,6
TADS Target Characteristics Parameter			
TADS Target Size	See Appendix	C	5
Target Contrast	See Appendix	C	5
Night Δ_t (target to background)	See Appendix	C	5
TADS Maximum Target Crossing Velocity	See Appendix	C	5
TADS Atmospheric Conditions Parameter			
TADS Atmospheric Conditions	During daylight the visibility is 12 km and scene illuminance is 1,000 to 100,000 lumens per square meter. For night (FLIR) operation, the atmospheric transmission is 85% per kilometer (8 to 14 microns).	U	4,5
TADS System Stabilization and Tracking Parameter			
TADS System Stabilization and Tracking	Provides the resolution and pointing accuracy required under the helicopter's vibration and translational and angular accelerations. Performance is not significantly degraded under the	U	4,5

Table 2-2. PARAMETERS THAT CAN AFFECT ASH TADS FLIR IMAGE QUALITY (Continued)

TADS System Stabilization and Tracking Parameter	Value	Classification	Reference
TADS System Stabilization and Tracking (Continued)	vibration and blast pressure environment caused by weapons firing.		
Linear Motion Compensation	Include in TADS	U	4,5
Image Motion Compensation	Is allowable to improve dynamic resolution	U	4,5
TADS Turret Slewing	Slewing rates at least to 1.047 radians/second (60°/second) in each axis and accelerations of at least 2.094 radians/second (120°/second)	U	4,5
TADS Tracking	0.5236 radian/second (30°/second)	U	4
TADS Controls and Displays Parameter			
Monitor Characteristics	Video monitor displays are compatible with specifications EIA-RS-343 and EIA-RS-330 and other requirements for the 875 and 525 horizontal scan rates, respectively, and has a minimum of 10 shades of gray ($\sqrt{2}$ brightness variation).	U	4**
TADS Vignetting/ Obscuration Parameter			
Vignetting/Obscuration	No vignetting is permitted for the FLIR and TV subsystems and there is no FOV cutoff due to obscurations within the TADS turret.	U	4,5

**These monitor characteristics were omitted in the revised version of this document.

2.4 IMAGE QUALITY ANALYSIS

The appendix shows the relationship between the number of picture elements across the target as a function of range for the three FOVs; the image motion in PELS/second versus range for the three FOVs; and image motion and angle rate for the three FOVs. It also discusses the effect of temperature on the FLIR lens distortion, and the expected temperature ranges for the target-to-background temperature differential, sky horizon temperatures, and sea temperatures.

2.5 REFERENCES

1. Issues Related to Helicopter Operating in Combat (U), D. L. Hall, October 1975, Northrop Corporation, Electro-Mechanical Division No. 7292 (SECRET)

2. AAH Remote Aerial Scout Designation Mode Operational Analysis (U), T. G. Baxter, July 1976, Northrop Corporation, Electro-Mechanical Division No. 7742 (SECRET)

3. Advanced Scout Helicopter Man-Machine Interface Investigation - Aviation Team, Human Engineering Applications Directorate, U.S. Army Human Engineering Laboratory, Aberdeen Proving Ground, Maryland, September 1975

4. TADS Prime Item Development Specification, DRC-DP-AAH-4020, April 1976

5. Prime Item Development Specification for TADS (U), DRC-DP-AAH-4020A, (Draft) 12 June 1976 (CONFIDENTIAL)

6. Prime Item Development Specification for Target Acquisition Designation (U), Northrop Corporation, Electro-Mechanical Division No. 7667, April 1976 (CONFIDENTIAL)

SECTION 3

FAST RATIONALIZED HAAR TRANSFORM

This section covers the basic definition of Haar functions, their extension to two-dimensional formats for image processing applications, and their expression in terms of matrices.

3.1 BASIC DEFINITIONS

Haar transforms provide the basis for all image processing techniques presented in this report. Like other transforms, they can assign quantitative measures to qualitative aspects of the original image, or replace an involved measurement technique by an easier and faster one. These measures in turn identify the important variables for processing image restoration and enhancement.

Haar transforms are also comparatively simple. Each transform component effectively multiplies the original function by either 0, +1, or -1. Furthermore, they combine the abilities of local transforms (e.g., Block transforms) to touch up given areas of a picture, with those of global transforms (e.g., Walsh transforms) to render broad comprehensive interpretation of data.

The general Haar function h(r,m,x) appears in Figure 3-1.

Sequency r bears a certain resemblance to frequency. Offset m ranges between 1 and 2^r. These mutually orthogonal functions can be rationalized by reducing all amplitudes $2^{r/2}$ to a common value of unity. A weighting function of 2^r, however, must then be included in either the forward or inverse transform.

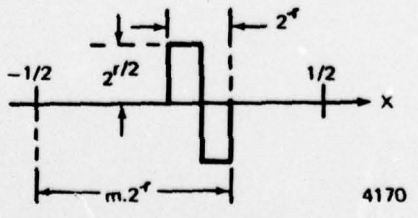

Figure 3-1. GENERAL HAAR FUNCTION h(r,m,x)

3.2 TWO-DIMENSIONAL FORMATS

Haar functions can be used to expand general one-dimensional waveforms. Two dimensional waveforms, such as image intensity distributions I(x,y) can similarly be expanded in a product series:

$$I(x,y) = \sum_{r,m,p,n} a_{rmpn}\, h(r,m,x)h(p,n,y) \tag{1}$$

$$a_{rmpn} = \int_{-1/2}^{1/2}\int_{-1/2}^{1/2} I(x,y)h(r,m,x)h(p,n,y)dxdy \tag{2}$$

While this applies to primary domain $-1/2 \leq x \leq 1/2$, $-1/2 \leq y \leq 1/2$, simple linear scale changes will qualify these relations for images of any finite extent.

A rationalized two-dimensional product h(r,n,x)h(p,n,y) appears as in Figure 3-2.

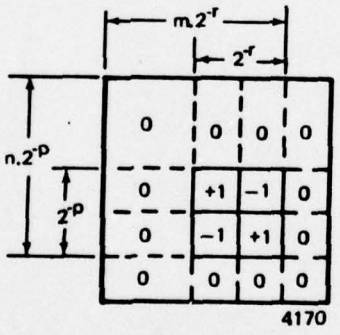

Figure 3-2. GENERAL TWO-DIMENSIONAL RATIONALIZED HAAR PRODUCT FUNCTION

When all such diagrams have been located in rectangular (r,p) coordinate space as in Figure 3-3, the resulting array represents the Haar image transform domain.

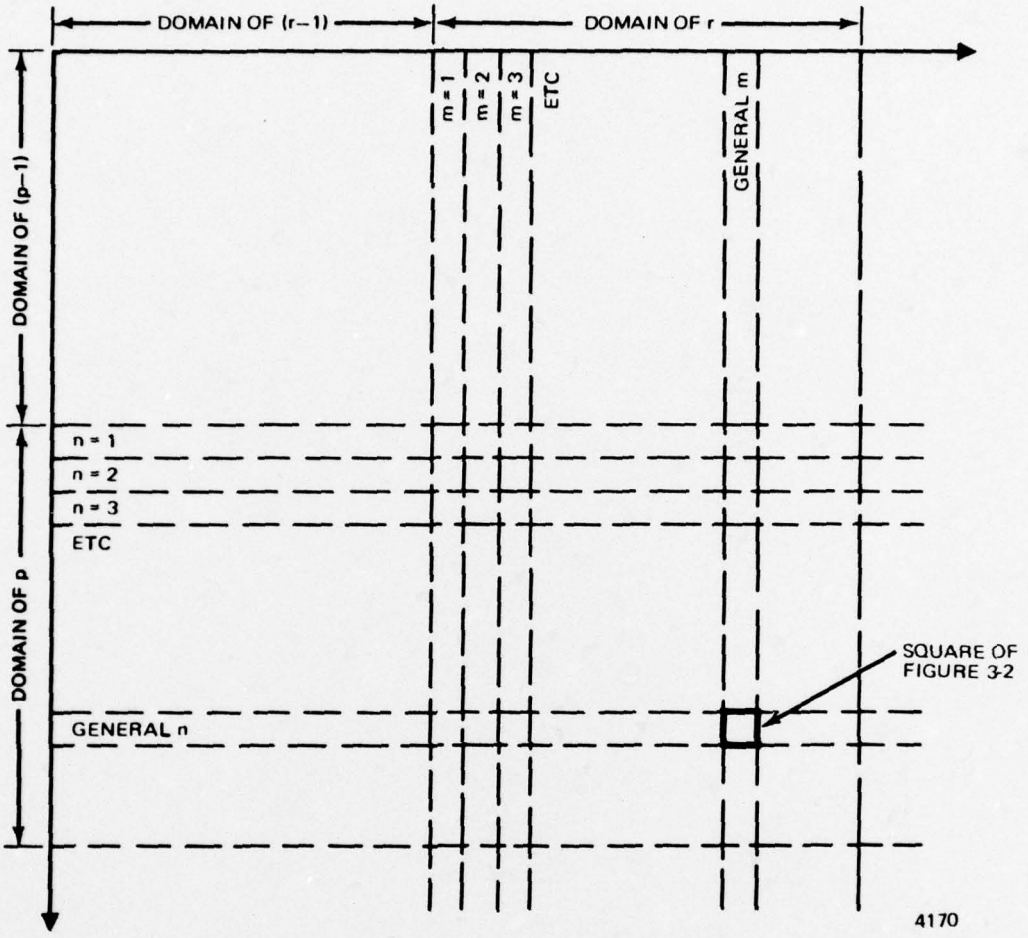

Figure 3-3. HAAR IMAGE DOMAIN

A detailed picture of the array is given in Figure 3-4.

3.3 MATRIX REPRESENTATION

Forward and inverse Haar transforms in equations (1) and (2) can also be expressed in terms of matrices. It should be noted that matrix expressions substitute discrete summation for integration in equation (2). With this proviso, continuous image distribution $I(x,y)$ reduces to the discrete expression $I(t\Delta x, l\Delta y)$ where Δx and Δy typically assume values smaller than the resolution spot size of the imaging system. Integers t and l span a range sufficient to cover maximum and minimum

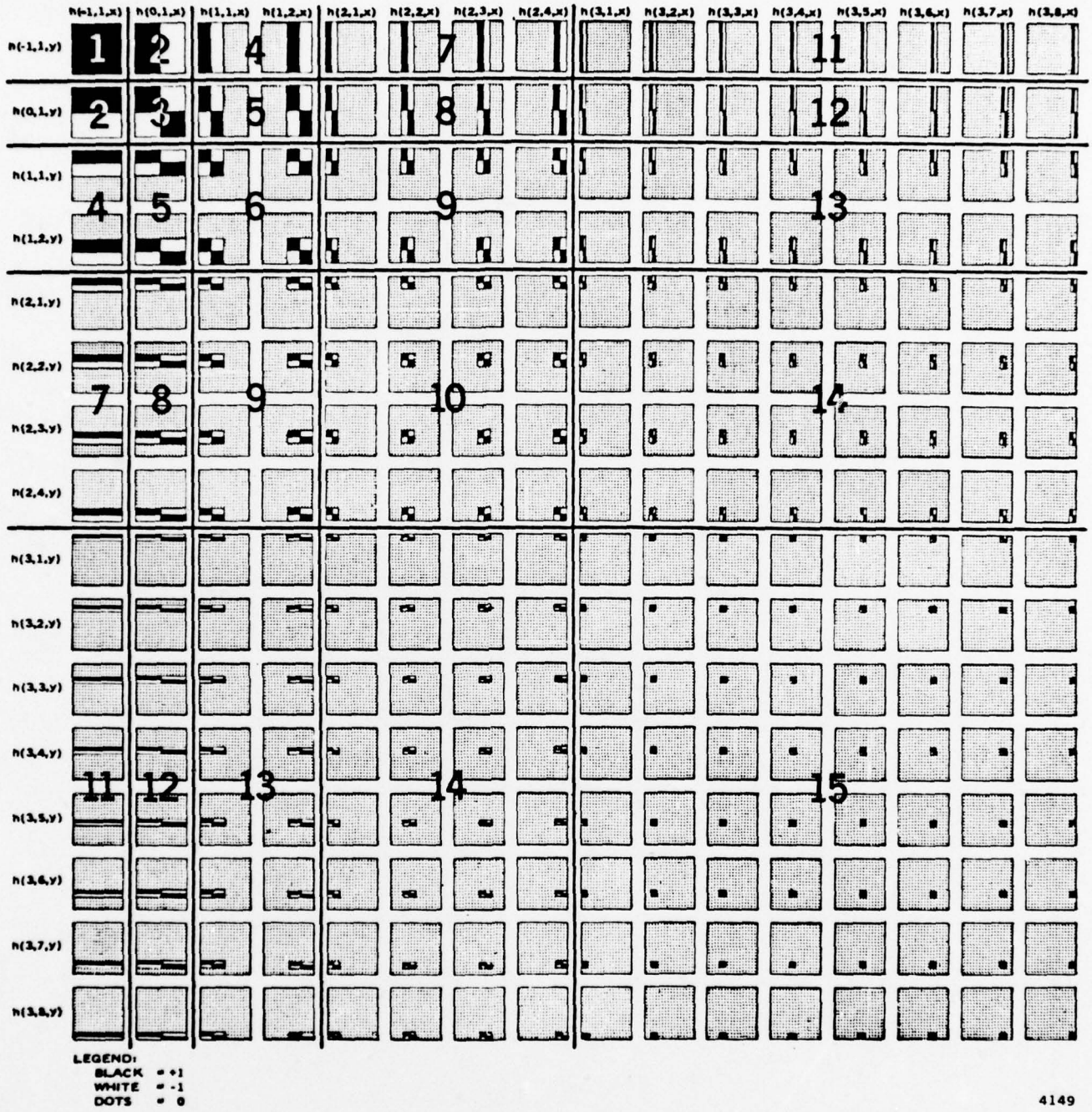

Figure 3-4. TWO-DIMENSIONAL RATIONALIZED HAAR FUNCTIONS

values of x and y. This expression in turn can be represented by the matrix $I_{t,1}$ or simply I.

Haar function h(r,m,x) reduces to the matrix h_{ts} where integer s designates successive Haar functions in a particular sequency and then moves on to the next sequency. Using only the first few sequencies in a rationalized format to clarify the illustration:

$$H_{\text{rationalized}} = \begin{bmatrix} 1 & 1 & 1 & 1 & 1 & 1 & 1 & 1 \\ 1 & 1 & 1 & 1 & -1 & -1 & -1 & -1 \\ 1 & 1 & -1 & -1 & 0 & 0 & 0 & 0 \\ 0 & 0 & 0 & 0 & 1 & 1 & -1 & -1 \\ 1 & -1 & 0 & 0 & 0 & 0 & 0 & 0 \\ 0 & 0 & 1 & -1 & 0 & 0 & 0 & 0 \\ 0 & 0 & 0 & 0 & 1 & -1 & 0 & 0 \\ 0 & 0 & 0 & 0 & 0 & 0 & 1 & -1 \end{bmatrix} = [h_{ts}]_{\text{rationalized}} \quad (3)$$

Expansion coefficient a_{rmpn} likewise reduces to matrix $[a_{sq}] = A$.

Equations (1) and (2) then convert to the matrix expressions

$$I = HAH^T \quad (4)$$

$$A = H^T I H \quad (5)$$

Because of the simplicity of (3) and the compactness of (4) and (5), the matrix approach will be preferred in general.

SECTION 4
IMAGE DESCRIPTORS

4.1 OVERVIEW

Although mean square error traditionally has been used as a fidelity criterion for most image coding techniques, there are some areas in which it does not compare well with human evaluation. As an example, mean square error does not make sense in the areas of image enhancement or blind restoration, and in most cases it cannot be obtained because no reference image is available. A quantification of the effect of various image enhancement and restoration techniques is required that agrees well with the human subjective evaluation and can be obtained easily from the image.

In order to facilitate the evaluation of images and image processing algorithms throughout the course of this study, a set of quantitative image descriptors has been developed. The descriptors basically summarize the information of the image by dividing it into two major categories, tone and activity. The tone of an image is governed by the diversity of the local ensemble averages of the gray levels of the image and is important in distinguishing objects within the scene. Activity is determined by the way the gray levels change from pel to pel and is a measure of how busy the scene is. In the Haar domain, these two features may be measured directly. Tone is equivalent to the variance of the dc terms, $a_{-1,1,-1,1}$, of each 16 x 16 pel block and activity is the total ac energy in the transform domain.

The division of image information into only two categories, tone and activity, is not sufficient for useful analysis, however. Two images may, for example, have comparable activity when one contains significant edges (outline of a tank, etc.) while the other contains only high-power white noise. For this reason, image activity is further subdivided into texture activity and edge activity.

Texture in the image is characterized by a series of repetitious gray level transitions (edges) that are usually, though not necessarily, of relatively low power. Edge information, on the other hand, is typified by a smaller number of gray level transitions, usually of higher power. These two characteristics are exhibited in the

individual sequency groupings of the Haar domain as broadly distributed power in the case of texture activity and as power spikes or singularities in the case of edge activity. By applying an edge criterion function to each transform coefficient within a sequency group, the activity (ac power) due to edge may thus be separated from the nonedge activity, which by default is due to texture.

4.2 USE OF DESCRIPTORS

The descriptors will be used to quantify the characteristics of images both before and after the application of various image processing algorithms. The resultant changes in the image descriptors can then be used to detect the net effect of processing on the image.

Changes in the descriptors can be presented in a more general format if the three individual descriptors are viewed as the components of a three-element descriptor vector. As an example, let T, E, and X be the values of an image's tone, edge activity, and texture activity descriptors, respectively, before processing. The image's descriptor vector, $\underline{ID}$, would be given by the column vector $\underline{ID} = [T, E, X]$. If T', E', and X' are the corresponding descriptor values and $\underline{ID}'$ is the descriptor vector after processing, the change in the image can be typified by the difference vector $\underline{D} = \underline{ID} - \underline{ID}'$.

Utilizing the difference vector $\underline{D}$ allows examination of the net amount of change given by $|\underline{D}|^2$, as well as the direction of change. Direction of change would be determined by the slopes of various projections of $\underline{D}$ onto planes of interest in image descriptor space. Measuring the direction of change is expected to be very useful as it should lend to the development of algorithms that, for example, affect edge more than texture.

4.3 DESCRIPTORS

Since the primary research tool for this sensor processor study performs the Haar transform on individual, nonoverlapping, 16 x 16 pel blocks, local descriptors must first be obtained for each block, and then combined to form global descriptors that apply to the entire image or areas of interest within the image. The definitions of the local descriptors and their rules of composition to form the global, or image, descriptors are presented here.

4.3.1 Local Descriptors

4.3.1.1 Local Tone - The local tone of a block is the dc term of its Haar transform. In the sensor processor's version of the rationalized Haar transform, the value of this term is equivalent to the average gray level of the image block. Let t_i be the local tone of the i^{th} block, $t_i \triangleq a_{rmpn}$, r = 1, m = 1, p = 1, n = 1. The term a^i_{rmpn} is in general the $rmpn^{th}$ term of the i^{th} block. In this case a^i_{rmpn} is the dc term.

4.3.1.2 Local Activity - The local activity of the i^{th} block is its ac energy. This is given by the sum of the squares of the ac terms of its Haar transform. Let c_i denote the local activity of block i,

$$c_i \triangleq \sum_{rmpn} (a^i_{rmpn})^2 - (a^i_{-1,1,-1,1})^2$$

The term c_i by itself is insufficient to characterize the information in block i. For this reason ac energy is divided into edge activity and texture activity.

4.3.1.3 Local Edge Activity - The local edge activity of the i^{th} block is the ac energy that satisfies the edge criterion function. In subjective terms, the edge criterion function says that if the power of an ac coefficient contributes more than its fair share to the total power of its sequency group, then that term is the result of an edge in the image domain. More specifically, if Ψ denotes the set of edge terms then

$$a^i_{rmpn} \in \Psi$$

if

$$\frac{(a^i_{rmpn})^2}{\sum_{mn} (a^i_{rmpn})^2} \geq \alpha^i_{rp} \; S^i_{rp}$$

where α_{rp} is the edge power threshold for the rp^{th} sequency group and S_{rp} is the relative entropy of the group. If $P(a^i_{rmpn})$ is the probability that a^i_{rmpn} will occur within the group, then

$$S^i_{rp} = \frac{\sum\sum_{mn} P(a^i_{rmpn}) \log_2 P(a^i_{rmpn})}{\log_2 (\text{number of terms in } rp^{th} \text{ group})}$$

The values of α_{rp} are shown in Table 4-1. As can be seen in the table, $\alpha_{rp} = \alpha_{pr}$. This reflects the assumption that horizontal and vertical edges are equally likely. The values of α_{rp} were chosen empirically, but approximate $1/1+K_{rp}$ where K_{rp} is the nominal number of Haar functions in the rp^{th} group to which a straight edge would contribute power. This approximate relationship for α_{rp} allows diagonal edges to be detected more readily.

The purpose of weighting α^i_{rp} with the group's relative entropy can be seen by examining the two representative histograms of coefficients of the rp^{th} group shown in Figure 4-1.

The power that the edge terms would require in order to differ significantly from the other terms is greater in the flat distribution of Figure 4-1B than in the distribution of Figure 4-1A. A good measure of the distribution flatness is its entropy. Its entropy is therefore used to weight the edge power threshold.

If we let e_i be the local edge activity, then

$$e_i \triangleq \sum\sum\sum\sum_{rmpn} (a^i_{rmpn})^2$$

if $\quad a^i_{rmpn} \in \Psi$

The terms $a^i_{-1,1,-1,1}$ can be excluded from the above expression by assuring that they will never satisfy the edge criterion function.

Table 4-1. GROUP EDGE WEIGHTING, α_{rp}

p \ r	−1	0	1	2	3
−1	NA	0	1/3	1/2	1/2
0	0	1	1/3	1/2	1/2
1	1/3	1/3	1/3	1/3	1/3
2	1/2	1/2	1/3	1/5	1/5
3	1/2	1/2	1/3	1/5	1/9

4170

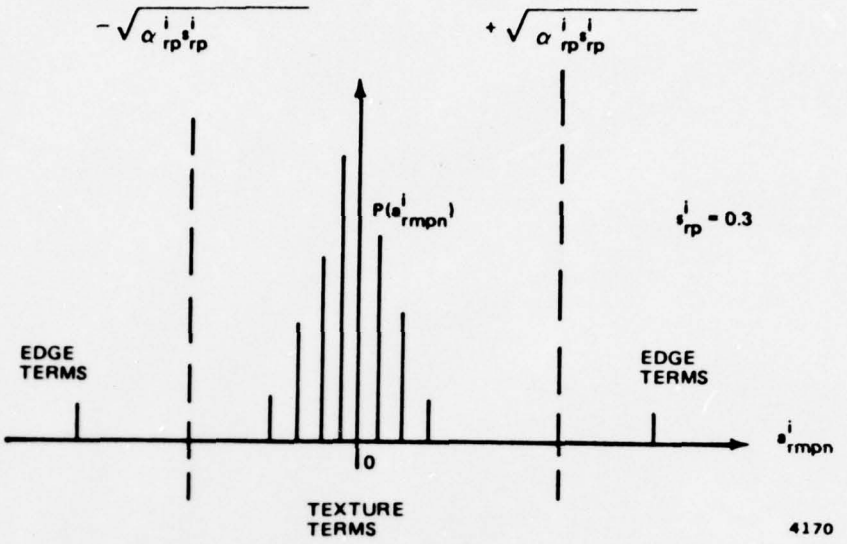

A – PEAKED DISTRIBUTION

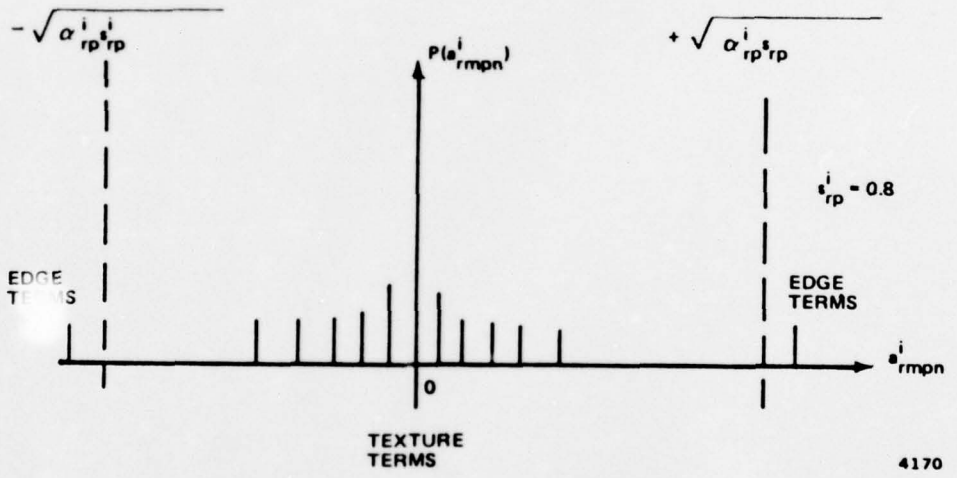

B – FLAT DISTRIBUTION

Figure 4-1. REPRESENTATIVE HISTOGRAMS OF COEFFICIENTS OF rp^{th} GROUP

4.3.1.4 Local Texture Activity - In this study, local texture activity is, by definition, the ac energy remaining in the block's Haar transform after all the edge terms have been removed. If $\times_i$ is the local texture activity for the i^{th} block, then

$$\times_i \triangleq \sum_{rmpn} \sum \sum \sum (a^i_{rmpn})^2 - (a^i_{-1,1,-1,1})^2$$

if $a^i_{rmpn} \neq \Psi$

4.3.1.5 Examples of Local Descriptors - Two sample images shown in Figure 4-2, "U.S.C. Girl" and "Moon," were selected for initial evaluation of the above descriptors. It was desirable for the test data set to be kept as small as possible for development purposes and yet be sufficiently diverse to exhibit a reasonable cross section of image characteristics. It is felt that the two selected images, Girl and Moon, provide enough local diversity individually and global diversity between each other to form a good initial test data set.

Each image consists of 256 x 256 pels that are subdivided into a 16 x 16 array of 16 x 16 pel blocks. The local descriptors were computed for each block of both sample images. The resultant arrays of local descriptors are given in Tables 4-2 through 4-5.

Examination of the arrays pertaining to the local tone of the Girl and Moon images (Table 4-2) shows that the results obtained are in good agreement with subjective evaluation. This is to be expected since the local tone is nothing more than the average gray level of the 16 x 16 pel block. Dark areas of each picture have a correspondingly lower local tone than bright areas. Subjective agreement is also good for local activity (Table 4-3). Busier areas of each picture have correspondingly higher values of activity.

Two blocks that both exhibit high activity and yet contain significantly different information are flagged by asterisks in Table 4-3A. The single asterisk value relates to a block containing the edge of the girl's face while the double asterisk value pertains to a block containing the flower. These two blocks provide good examples of edge and texture. The local texture activity values of the same two

U.S.C. GIRL

MOON

Figure 4-2. SAMPLE IMAGES

Table 4-2A. LOCAL TONE ACROSS GIRL IMAGE

48	50	54	48	47	34	24	58	97	88	55	69	61	110	134	124
47	51	54	48	52	47	97	156	144	154	152	91	65	112	125	113
48	51	55	59	55	95	138	130	108	81	101	141	100	112	101	79
48	52	54	56	62	75	75	43	31	22	34	114	129	116	102	91
47	52	53	49	63	74	82	58	38	46	75	88	121	93	90	87
45	51	53	50	54	42	63	59	44	49	44	71	101	86	77	82
44	50	51	47	50	63	108	87	48	51	37	75	118	84	74	72
43	48	49	45	47	106	147	127	115	73	61	121	124	87	76	75
42	46	47	44	46	79	104	102	102	88	103	111	131	97	75	77
39	44	45	43	45	53	122	114	87	71	106	105	129	86	67	78
34	35	39	37	39	36	71	81	47	59	105	119	121	104	108	111
24	25	35	25	59	93	93	70	66	49	61	88	82	90	99	96
58	64	51	81	102	101	79	74	59	75	72	55	66	89	94	87
47	49	44	70	86	87	74	48	32	29	53	25	31	32	52	69
10	13	35	48	50	76	110	105	18	86	202	146	38	26	24	81
10	14	40	69	39	59	75	94	139	147	158	205	180	108	19	46

Table 4-2B. LOCAL TONE ACROSS MOON IMAGE

147	136	131	135	127	134	131	142	139	142	147	142	136	151	160	141
147	140	139	133	126	128	137	134	137	147	148	145	140	141	147	141
149	150	154	108	174	129	136	138	136	144	123	141	148	142	157	162
154	154	160	123	148	139	132	137	143	178	85	84	151	148	155	165
154	154	151	151	148	135	131	128	122	174	121	77	144	153	159	161
140	143	136	140	140	128	142	109	112	110	159	103	152	164	157	159
143	139	131	132	128	119	124	111	111	120	129	142	154	162	165	163
137	136	128	127	127	122	119	101	104	118	116	129	151	148	147	154
135	134	129	118	119	113	115	87	95	105	125	128	145	156	162	162
131	123	124	115	114	116	105	101	101	108	114	130	144	149	146	150
132	119	126	122	113	113	103	90	107	106	105	115	129	132	138	155
134	136	133	128	113	125	101	71	104	105	109	118	116	128	149	161
134	137	134	123	119	135	114	67	81	99	103	125	121	126	147	154
131	129	120	115	120	133	121	30	37	96	101	110	114	118	136	147
132	127	108	103	100	105	123	75	44	86	109	114	114	120	143	149
126	123	110	100	107	105	102	97	85	90	120	120	123	129	139	144

Table 4-3A. LOCAL ACTIVITY ACROSS GIRL IMAGE

277	286	266	212	232	358	179	5884	7620	8595	2604	416	1160	1255	691	849
290	301	266	236	216	1003	10502	3507	2218	2347	5654	4540	1912	893	950	920
291	314	289	224	367	3751	3478	4971	4285	3045	1692	8728	2765	988	1259	501
319	297	277	239	1064	2249	6057	3106	1199	1010	929	5896	1208	919	817	579
265	301	276	221	1149	2355	2362	2659	1448	1158	3584	3142	1371	1191	763	433
248	287	237	210	511	3946	2419	1704	2070	1074	1046	2874	1928	1047	645	672
249	266	187	186	187	4895	6164	5965	3269	1284	1096	4779	905	1175	631	380
211	229	193	202	224	4976*	3311	2937	3415	1213	2351	2548	870	1050	581	510
221	225	236	171	265	3098	5116	4424	2107	1269	2666	991	830	1046	459	524
180	244	176	198	194	2254	4275	3591	1735	1023	2128	812	1002	1017	771	862
706	195	166	170	171	948	8734	7103	603	688	6024	2069	1056	835	725	901
2443	2096	234	637	7592	5334	2393	6076	3364	3764	2174	2222	8289	4637	738	759
2006	1880	1516	5775	1186	778	3598	2923	3477	2387	799	1510	3839	5041	3147	715
2016	41.	1290	2623	4038	1705	1427	2287	2201	7140	9111	582	197	340	3346	2439
131	137	1191	310	838	3194	5296	6259	4879	23606	4516	16796	6608	445	521	2040
262	137	1727	675	431	3779	2701	7222	12652	9089	8514	2665	15141	23541	130	2173

Table 4-3B. LOCAL ACTIVITY ACROSS MOON IMAGE

1282	3587	1339	1541	1734	1174	1563	1380	2368	2667	2059	2241	3264	2536	4499	9975
1307	5575	850	2331	2068	1187	1537	2056	1050	1641	1083	1467	1174	1269	911	2026
1062	975	1472	5850	8137	1282	3202	1361	1876	1749	1659	1581	1905	2740	1255	3521
721	714	1002	5713	4266	916	1426	2227	2139	2257	5259	4764	918	1157	1648	1133
1732	2475	1037	2283	1045	1354	1021	1200	1939	3153	6454	3049	1299	991	1580	1457
2761	2681	5660	2425	1620	4759	1133	1880	2580	2927	2706	2130	1753	1224	2274	2025
941	1404	3274	5127	6809	1689	1778	1842	1544	974	1242	860	1228	1107	1400	1192
3641	1738	2487	1958	960	1597	3754	1960	1506	1389	1927	1756	1741	834	1339	2576
4548	1763	2381	2648	1094	1384	2386	3487	1403	1214	1132	1408	943	739	670	1532
2937	4435	2508	2190	1075	1156	2984	3186	1423	1439	1318	769	489	1571	882	941
1119	1852	3204	1916	2360	1349	2660	2606	1830	4239	1221	1554	352	1599	1344	900
1072	1904	1322	1468	1678	1441	1472	2196	1380	3145	989	1089	1479	847	1139	1202
3639	1509	1057	1910	2126	1459	1467	1812	2276	831	992	1312	1389	1041	856	1214
857	1513	1727	2452	1896	2943	5555	3698	2447	1180	1608	1679	1307	1886	1364	1010
1391	989	3001	8216	4912	4921	4661	4479	3900	3325	941	1567	1034	1098	1311	818
1280	1505	1173	2106	1328	3774	3152	3082	2587	2506	912	1217	899	1334	1159	915

Table 4-4A. LOCAL TEXTURE ACTIVITY ACROSS GIRL IMAGE

91	65	117	75	85	54	41	998	1903	2044	571	215	433	624	406	490
77	135	119	95	69	250	5312	1896	1858	1305	3294	1886	721	482	540	431
65	146	107	70	179	2607	2487	3800	2191	1530	1056	4998	960	522	695	298
157	79	136	117	338	1483	2556	1916	771	615	485	3484	792	593	406	265
82	114	139	74	340	1302	1412	1705	846	770	2541	2026	626	528	337	243
93	86	74	66	222	1227	1164	1130	889	550	419	1578	548	431	292	376
104	79	65	58	78	2932	3715	3951	2294	651	614	2060	436	514	315	199
68	70	65	68	63	1109*	2064	1778	1277	629	1443	1026	532	446	282	233
63	85	120	61	135	1062	3350	2411	950	677	1653	562	456	571	185	305
59	82	69	58	77	1410	2487	2074	848	662	971	549	583	613	350	431
152	31	31	40	72	532	5361	3771	253	318	3590	1205	549	399	409	544
1600	613	71	148	2389	2138	952	3404	571	1619	1117	739	4345	2374	390	479
896	809	858	2974	672	448	1240	1880	1938	1450	398	403	1415	2806	1529	408
853	81	393	1137	2312	1017	571	1075	1171	2999	3128	301	54	122	1425	1096
7	9	224	127	275	1916	4164	3592	2719**	14675	2985	7608	887	167	184	1154
29	8	736	312	86	2749	1794	5131	4236	6571	6141	1979	5742	8394	5	589

Table 4-4B. LOCAL TEXTURE ACTIVITY ACROSS MOON IMAGE

829	1844	810	1125	1246	771	962	856	997	1707	1434	1606	1754	1700	2676	5038
787	2115	622	1345	1520	643	1243	1440	764	1169	731	1128	769	949	657	1339
667	615	607	2508	3364	886	1736	1092	1325	1160	782	914	1417	1727	746	1187
493	476	552	3039	2682	658	1084	1205	1248	1304	2482	1699	558	741	1093	814
812	1469	541	1192	631	1021	684	679	1128	883	2242	766	803	612	1045	1014
2067	1773	4090	1403	1009	2365	595	1039	1081	1058	1487	951	1195	590	1235	1350
622	877	1985	3607	5783	1060	1103	1187	1068	609	809	524	690	651	644	744
1932	1138	1341	1519	635	975	1893	1227	852	865	1304	984	1330	488	593	1413
1673	1222	1517	2186	632	939	1362	1817	1045	741	866	986	574	459	398	756
1389	2512	1631	1698	749	776	2082	1835	957	1019	868	515	223	880	486	644
577	1239	1836	1256	1145	768	1855	1650	1219	2373	725	795	352	574	719	597
792	1289	839	1046	1326	770	791	1185	853	1921	650	625	995	517	585	731
1294	870	667	1110	1234	839	610	1192	1157	567	672	689	892	835	419	631
487	894	966	1692	1250	1614	3107	1921	1273	707	917	1142	868	1151	724	606
862	618	1948	4803	2815	3365	3528	2877	2118	2080	570	1013	719	632	724	623
952	731	689	1875	780	2161	1585	1800	1611	1526	563	786	541	828	757	612

Table 4-5A. LOCAL EDGE ACTIVITY ACROSS GIRL IMAGE

186	221	149	137	147	304	138	4886	5717	6551	2033	201	727	631	285	457
213	166	147	141	147	753	5190	1611	360	1042	2360	2654	1191	411	410	439
226	168	182	154	188	1144	991	1171	2094	1515	636	3730	1805	466	564	293
162	218	141	122	726	766	3501	1190	428	395	444	2412	416	326	411	314
183	187	137	147	809	1053	950	954	602	388	1043	1116	745	663	426	190
155	201	163	144	289	2719	1255	574	1181	524	627	1296	480	616	353	296
145	187	122	128	109	1963	2449	2014	975	633	482	2719	469	661	316	181
143	159	128	134	161	3867*	1247	1159	2138	584	908	1522	338	604	299	277
158	140	116	110	130	2036	1766	2013	1157	592	1013	429	374	475	254	219
121	162	107	140	117	844	1788	1517	887	361	1157	263	419	404	421	371
548	164	135	130	99	416	3373	3332	350	370	2434	864	507	436	316	357
843	1483	163	489	5203	3196	1441	2672	2793	2145	1057	1483	3944	2263	348	280
1200	1071	658	2801	514	330	2358	1043	1539	937	401	1107	2424	2255	1618	597
1163	336	897	1486	1726	688	856	1212	1030	4141	5983	281	143	218	1921	1343
124	128	967	183	563	1278	1132	2667	2160**	8931	1531	9188	5721	278	340	886
233	129	991	363	345	1030	907	2091	8416	2518	2373	686	9399	15147	125	1584

Table 4-5B. LOCAL EDGE ACTIVITY ACROSS MOON IMAGE

453	1743	529	416	488	403	601	524	1371	960	625	635	1510	836	1823	4937
520	3460	228	986	548	544	294	616	286	472	352	339	405	320	254	687
395	360	865	3342	4773	396	1466	269	551	589	877	667	488	1013	509	2334
228	238	450	2674	1584	258	342	1022	891	953	2777	3065	360	416	555	319
920	1006	496	1091	414	333	337	521	811	2270	4212	2283	496	379	535	443
694	908	1570	1022	611	2394	538	841	1499	1869	1219	1179	558	634	1039	675
319	527	1289	1520	1026	629	675	655	476	365	433	336	538	456	756	448
1709	600	1146	439	325	622	1861	733	654	524	623	772	411	346	746	1133
2875	541	864	462	462	445	1024	1670	358	473	266	422	369	280	272	776
1548	1923	877	492	326	380	902	1351	466	420	450	254	266	691	396	297
542	613	1368	660	1215	581	805	956	611	1866	426	759	500	1025	625	393
280	615	483	422	352	671	681	1011	527	1224	339	464	484	330	554	471
2345	639	390	800	892	620	857	620	1119	264	320	623	497	206	437	583
350	619	761	760	646	1329	2448	1777	1174	473	691	537	439	735	640	404
439	371	1053	3413	2097	1556	1133	1602	1782	1245	371	554	315	466	587	195
328	774	484	231	548	1613	1567	1282	976	980	349	431	358	506	402	303

blocks are similarly flagged in Table 4-4. Note that the value of texture activity is much greater for the flower sector than for the edge sector. Table 4-5 shows that the edge activity is likewise isolated in the edge sector.

4.3.2 Global Image Descriptors

Obtaining global descriptors of tone, edge activity, and texture activity requires a suitable combination of the quantities computed on the subpictures of the image. Since the edge and texture activity add up to local activity numerically, only the results of local tone and activity will be developed herein. The rules for the combination of local edge and texture activity will be equivalent to those of local activity.

The local tone and activity have been computed on all of the 256 blocks of sample images girl and moon. The arrays of the local values of tone and activity were given in Tables 4-2 and 4-3. A single number must be computed from each of the arrays that characterizes the basic differences between the two images. To aid in the comparison of the images, some first order statistics of the local arrays were computed as shown in Table 4-6.

Table 4-6. STATISTICS OF LOCAL TONE AND ACTIVITY

	Girl	Moon
Local Tone		
Mean	73	127
Minimum	10	30
Maximum	205	178
Standard deviation	35	22
Local Activity		
Mean	2,367	2,065
Minimum	130	489
Maximum	23,606	9,975
Standard deviation	3,189	1,391

4.3.2.1 Image Tone - As can be seen from Table 4-6, the mean of the local tone (average brightness) is greater for moon than for girl. Subjective evaluation, however, indicates that the girl image has the most tone. In agreement with the concept that tone and brightness should be different quantities on any given picture, the standard deviation of the local tone is taken as a measure of the global, or image, tone. Let the image tone be denoted by T, then

$$T \triangleq \sigma_{t_i} = \left(\frac{\sum_i (t_i - B)^2}{N - 1} \right)^{1/2}$$

where t_i is the local tone of the i^{th} block, B is the average brightness of the image, and N is the number of 16 x 16 pel blocks in the image. The source of the difference in standard deviations of the local tone of the two images can be seen readily by examining the histograms of local tone shown in Figures 4-3 and 4-4.

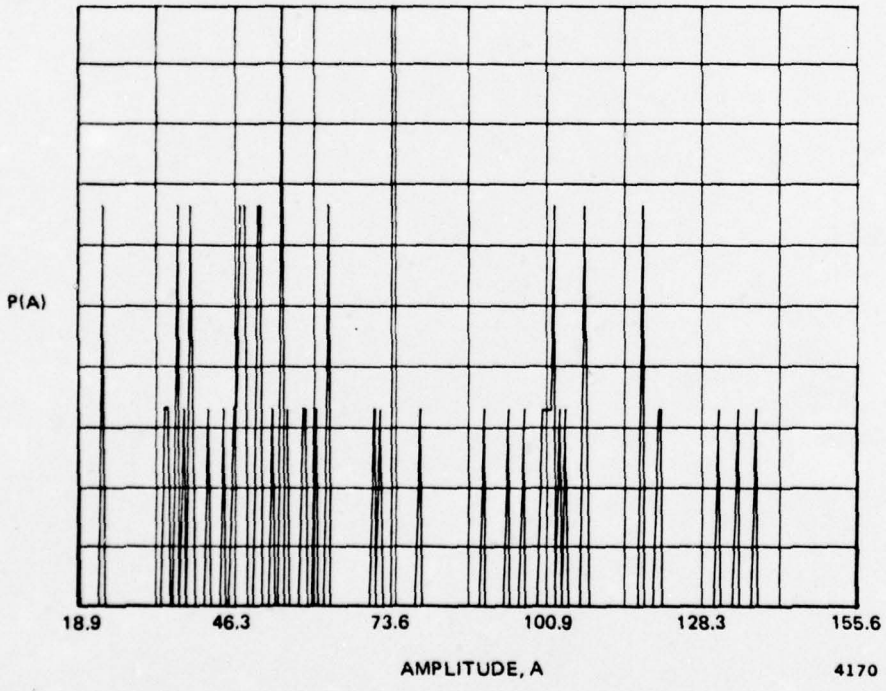

Figure 4-3. HISTOGRAM OF LOCAL TONE OF GIRL

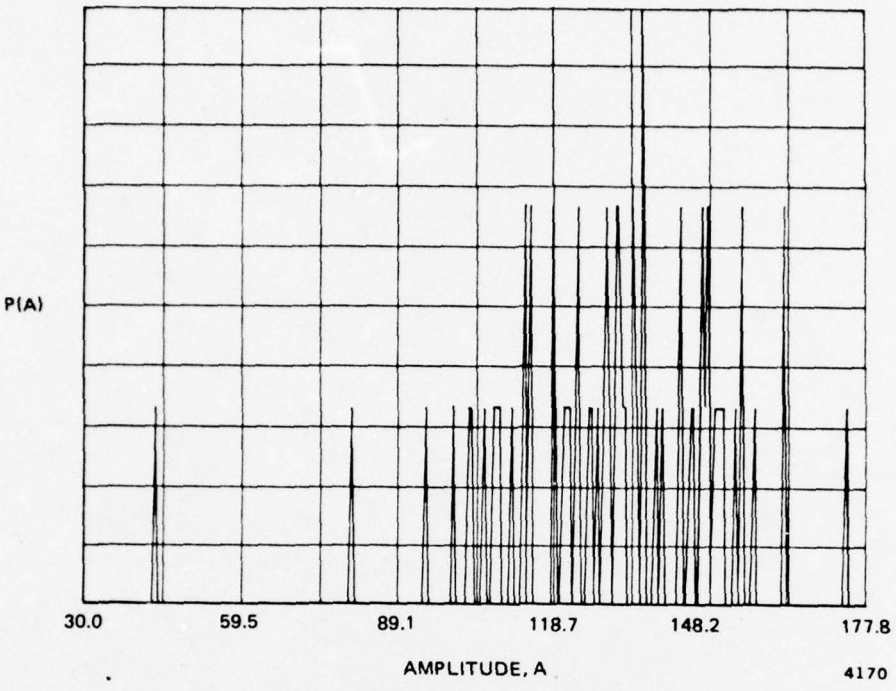

Figure 4-4. HISTOGRAM OF LOCAL TONE OF MOON

The preceding expression for image tone exhibits the following characteristics: When the local tone of each image block is approximately equal, i.e., the total picture is of uniform average intensity, the image tone is near zero. When the local tone changes significantly from block to block, the image tone is large.

4.3.2.2 Image Activity - A comparison of the statistics of the local activity of the girl and moon images (Table 4-6) reveals a significant difference in their standard deviations. The standard deviation of the local activity is not, however, taken as a measure of image activity. The reason for this decision becomes clearer when we consider the following example: In a given image assume that each 16 x 16 pel block contains either sufficient edge or texture information to give it a local activity of a_o, a constant. Each block may be completely different from its neighbors; the only similarity is their local activity. If the standard deviation of the local activity were the measure for image activity, the image activity would be zero. But, if one half of the blocks of the above image were changed to a uniform gray, i.e., made to contain no a-c energy, the standard deviation of the local activity would increase. Such a result is counterintuitive to a measure of image activity.

The measure to be used for image activity is the mean of the local activity. Image activity thus measured would rise and fall in agreement with subjective evaluation in the example given.

The standard deviation of the local activity does, however, impart some information about the total image. This parameter is dubbed "image diversity" but, along with image brightness, is not presently considered a necessary element of the global image descriptors. Further evaluation of the descriptors on a larger set of images may alter this conclusion.

Examination of Table 4-6 shows that the girl image is about 15 percent more active than the moon image. Let A denote the global, or image, activity,

$$A \triangleq \frac{1}{N} \sum_i a_i$$

where a_i is the activity of the i^{th} block. Similar expressions apply for X, the image texture activity and E, the image edge activity; i.e.,

$$X \triangleq \frac{1}{N} \sum_i x_i$$

$$E \triangleq \frac{1}{N} \sum_i e_i$$

where x_i and e_i are the local texture and edge activity respectively.

The statistics of the division of local activity into edge and texture activity for the two sample images are shown in Table 4-7.

Table 4-7 shows that the global texture activities of the two images are comparable but the girl image displays more edge activity. This is in good agreement with initial subjective analysis.

Table 4-7. STATISTICS OF LOCAL EDGE AND TEXTURE ACTIVITY

	Girl	Moon
Local Edge Activity		
Mean	1,191	850
Maximum	15,147	4,937
Minimum	99	195
Standard deviation	1,754	737
Local Texture Activity		
Mean	1,176	1,214
Maximum	14,675	5,783
Minimum	5	223
Standard deviation	1,635	776

4.3.2.3 Global Descriptor Vector - The three global features used as image descriptors are T, image tone; E, image edge activity; and X, image texture activity. These three descriptors are defined to be the components of the image descriptor vector, $\underline{ID}$. $\underline{ID} \triangleq [T,E,X]$. Thus, the descriptors of an image define a point in a three-dimensional image descriptor space. The concept of the image descriptors describing points in space will prove useful in describing the distances and directions between the image descriptor vectors of original and processed images.

4.4 SUMMARY AND CONCLUSIONS

A vector of image descriptors has been developed. The components of the vector correspond to the image tone, edge activity and texture activity. The sum of edge and texture activity results in the image activity in general. The image activity can be obtained directly from the image by ensemble averaging the local a-c energy of the image blocks of interest. The separation of local activity into edge and texture activity is accomplished by studying the statistics of groups of coefficients in the two-dimensional Haar domain.

The image tone is obtained by computing the standard deviation of the local tone (brightness) of the image blocks of interest.

The descriptors, as defined, provide valuable measures of the qualitative differences and similarities of the two test images. However, as the program progresses and an increasing set of FLIR images are evaluated, some of the aspects of the descriptor set may have to be changed. For example, at the local level, the set of group edge weights, α_{rp}, used in the edge criterion function may have to be optimized to better suit FLIR image characteristics. At the global or image level, features such as image diversity or brightness may prove to contain vital information and therefore be included as components of the descriptor vector.

The use of general vector concepts in the comparison of the image descriptors of different images is expected to provide insight into not only the magnitude of change induced by the application of an image processing algorithm, but to the direction, or quality, of change as well.

SECTION 5
EXPERIMENTAL PLAN

This section describes the basic plan or approach for conducting the various experiments and computer simulations required to gather test data. It is hoped that this data will provide an insight, and ultimately a solution, to the problems associated with present day imaging FLIR systems.

5.1 GENERAL APPROACH

All experiments will be conducted utilizing either one of two system configurations: (1) Northrop's two-dimensional sensor processor in conjunction with an instrumentation system, or (2) computer simulation on Northrop's Data Processing Center IBM 370 computer.

The experimental setup utilizing the two-dimensional sensor processor is preferred because (1) it processes imagery in near real time, and (2) it has a CRT display. These two capabilities provide the system with features that model more closely the Advanced Scout Helicopter (ASH) visionics. For example, image motion and psychovisual effects of images displayed on a CRT monitor (scan format, scan rate, etc.) would be encountered in the operation of the FLIR system installed on ASH.

5.1.1 Two-Dimensional Sensor Processor

The majority of the experiments will be conducted on the experimental setup depicted in Figure 5-1. The setup includes Northrop's two-dimensional sensor processor shown in Figure 5-2, an instrumentation subsystem, and assorted ancillary equipment.

The two-dimensional sensor processor has the capability of accepting both static imagery in the form of photographic transparencies, or dynamic imagery recorded on a one-inch video tape. (Recorded video must be in RS170, 525-line, 30-frame-per-second format and be compatible with the IVC 800A tape recorder/reproducer.)

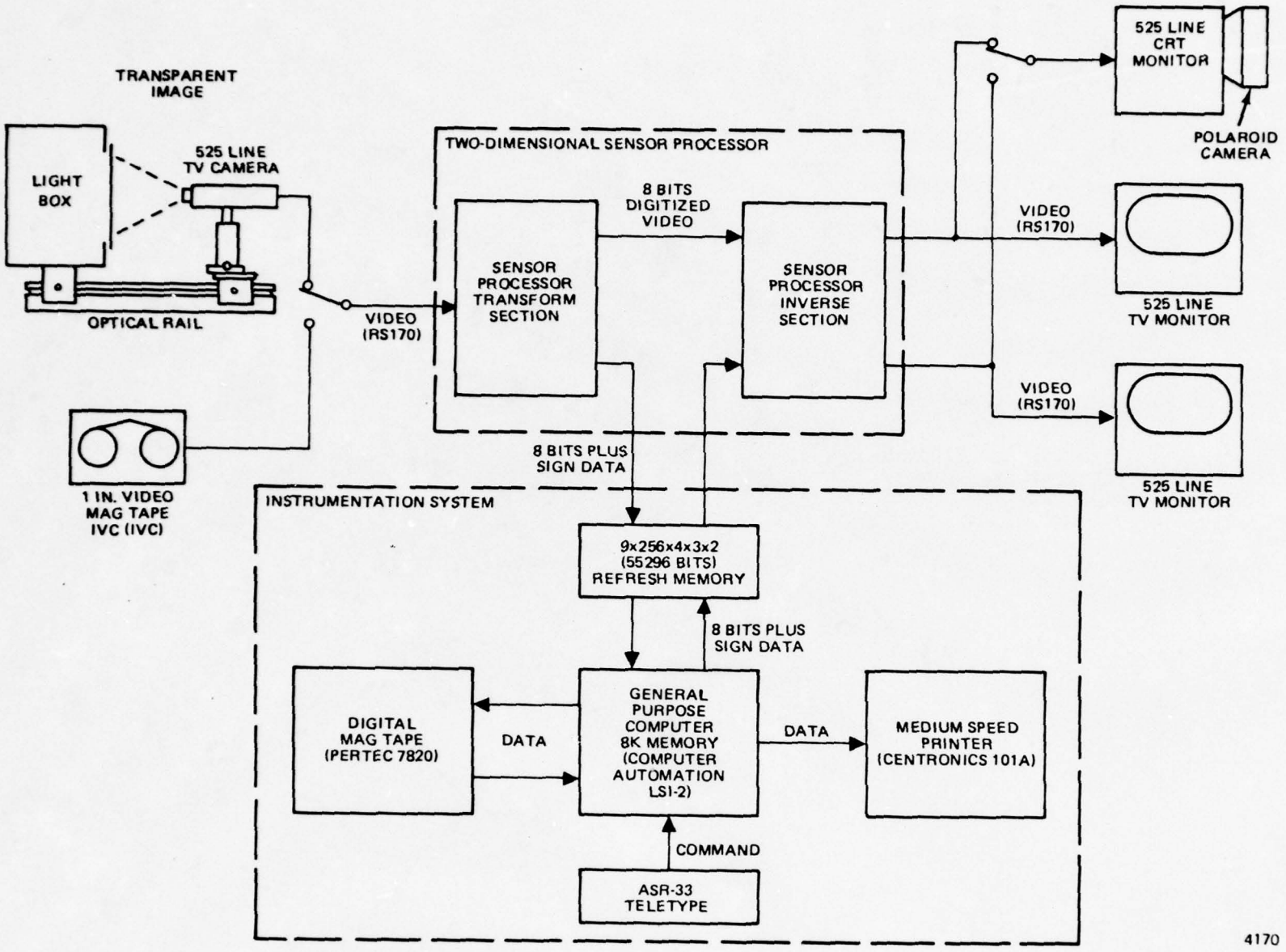

Figure 5-1. EXPERIMENTAL TEST CONFIGURATION

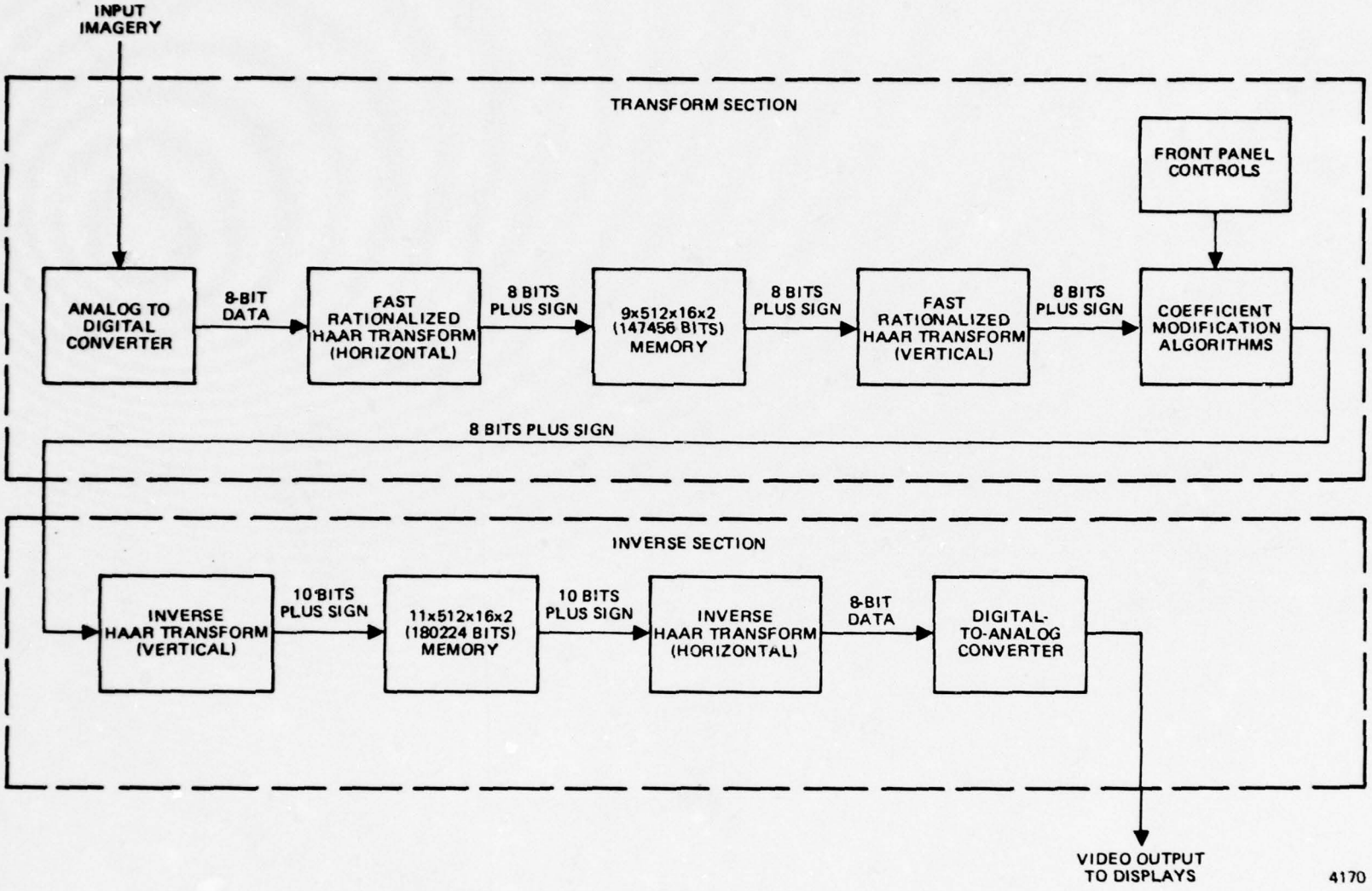

Figure 5-2. TWO-DIMENSIONAL SENSOR PROCESSOR FUNCTION FLOW DIAGRAM

The transform section of the two-dimensional sensor processor accepts the video signals from either the video camera or the video tape unit, and digitizes it linearly to an 8-bit resolution (256 shades of gray). The digitized video is then converted into the Haar domain (in two dimensions) by using a fast rationalized Haar transform. The resultant transform coefficients can now be altered by a limited number of hardware implemented algorithms by using the processor's front panel controls.

The transformed imagery, whether modified or not, is accepted by the instrumentation subsystem. It includes a refresh memory, a minicomputer, a digital magnetic tape transport, and a medium speed printer. The instrumentation system provides the capability to record, refresh, and input the transform coefficients of the image. Recorded coefficients will be analyzed off-line to describe the statistical contents of an image. The resultant descriptors can then be used for analysis of imagery data and for evaluating the effects of applied algorithms. They can also serve as a basis for assessing the progress and achievements reached in development programs.

The refresh memory between the sensor processor and the minicomputer provides the capability to snatch a limited area of the transformed image (approximately 3 percent of the total image). This data may be input to the minicomputer for modification beyond the present capacity of the processor front panel controls. Such modification is performed by the minicomputer's software and is not in real time. The portion of the image modified by the minicomputer is then stored and recirculated in the refresh memory to refresh the TV monitors.

The inverse section of the two-dimensional sensor processor converts the Haar transform of the image back into a video signal that is displayed on the TV monitors.

Two TV monitors are provided to enable a person to view both the original image and the modified image simultaneously for comparison.

Either the original or modified image may be displayed on a small 5-inch CRT monitor with a photograph camera attached. This allows for obtaining snapshots of test images.

5.1.2 Computer Simulations

Some computer simulations will be required where the hardware limitations of the two-dimensional sensor processor preclude the development of some concepts otherwise preferred. The IBM 370 computer will also be utilized to solve more complex mathematical problems such as obtaining a Haar expression or approximation of a blur that is expressed in the Fourier domain.

The computer simulation setup depicted in Figure 5-3 includes an IBM 370, centrally located at Northrop's Electronics Data Processing Center, with remote access terminals (RAX) located at each corporate division.

Simulation programs and digitized imagery are input to the simulation setup at the 370 computer via a magnetic tape unit. The various algorithms are entered at the RAX terminals. Data outputs resulting from application of algorithms to imagery data, including status and check comments, are directed to the RAX terminal printer for evaluation. Data outputs are also directed to the IBM magnetic tape unit for subsequent off-line composition into photograph form. Intermediate results of the simulations may also be input to the sensor processor via the sensor processor instrumentation subsystem's digital tape transport (Figure 5-2). This allows "quick look" examinations of processed imagery on a CRT display.

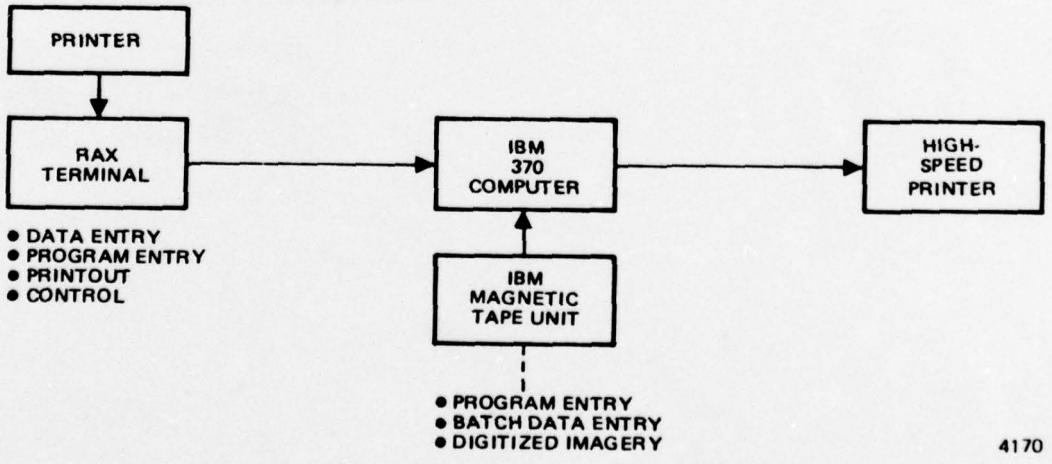

Figure 5-3. COMPUTER SIMULATION SETUP

5.2 EXPERIMENTAL TASKS/STUDIES OVERVIEW

The objectives, conceptual solutions and generalized experimental approach to principal areas in which Haar transform processing can improve FLIR imaging are detailed in the following paragraphs. Many of the original concepts were developed under Northrop's CY 75 and CY 76 Independent Research and Development programs. Specific areas covered include autofocus, autodeblur, image enhancement, adaptive signal processing and data compression.

5.2.1 Autofocus

5.2.1.1 Objective - Because severe demands are placed on a two-man helicopter team, the need for manual FLIR image refocusing can pose a formidable problem. FLIR defocusing arises from continual changes in observation range as well as from other incidental causes. Automatic refocusing offers a means to combat these tendencies and relieve part of the manpower burden. The apparatus should sense the defocus condition and produce a corresponding error signal for automatic correction. This signal might be used only on a brief periodic basis, to minimize mechanical wear.

5.2.1.2 (See addendum to this report)

5.2.1.3 Experimental Approach - Experimental procedure generally consists in varying the focus of the input TV camera and noting the effect at the output of the Haar transform processor. The camera may be directed at a test pattern which emphasizes a particular resolution spot size. This pattern should extend only over a single 16-by-16 pel subsection of the image plane.

Under preliminary in-focus conditions, the boundary limits derived from the processor output should be checked against the pattern spot size. For completeness, all Haar coefficient amplitudes should be measured.

The camera can then be defocused by varying amounts to either side of the ideal setting and the coefficients again measured. Graphs of variations of meaningful Haar coefficients with different defocus settings can then be constructed. These should have the general shape of Figure 5-4 (see addendum). They will effectively convert the dither sensitivity of the system into an equivalent (non-linear) transfer function about which a corrective feedback loop may be designed.

Real photographic scenes can then be substituted for the test pattern, and the above process repeated. Here, however, the object will be to determine whether different scenes generate the same type graph as that illustrated in Figure 5-4 (see addendum), so that a given corrective design might serve a large variety of possible situations. To this end, five photographs showing strong mutual diversity might be selected.

5.2.2 Autodeblur

5.2.2.1 Objective - Pertinent problem areas include atmospheric blurring, depth of field and motion blur. Each one can seriously degrade image resolution.

Atmospheric blurring can arise from haze, thermal gradients, clear air turbulence, and related causes. These produce dynamically changing random refractive index gradients that degrade the spatial coherence of wavefronts radiated by the object.

Depth-of-field blurring concerns the spread of slant ranges to different parts of a large obliquely viewed target, and the inability to bring them all into focus simultaneously. Low altitude reconnaissance typifies this situation.

Motion blur refers both to jittered and smeared images. Even if perfect correction were performed for smeared images, the extremely rapid motion associated with smeared images does not permit the eye-brain combination to view them comprehensively in real time. Because of this limitation, smearing will not be considered at this time. Jittering due to underdamped gyros or servo stability problems, however, may benefit from Haar transform concepts.

5.2.2.2 Atmospheric Blur -

5.2.2.2.1 Concept - Atmospheric blurring effectively convolves unknown blur function $b(x,y)$ with ideal image $i(x,y)$. Representative shapes of $b(x,y)$ include a pillbox, a cone or any hill-like form which extends over several pels. This extent, or footprint, is typically small compared to the overall image dimensions. Convolution uses this footprint like a broad brush, to trace out pictorial details in $i(x,y)$. The coarsened result is the blurred picture. As footprint size increases, therefore, the blurring becomes progressively worse.

Autodeblurring consists in identifying $b(x,y)$, and using the information to cancel its effect. Identifying $b(x,y)$ however requires some procedure for separating it from $i(x,y)$, since the two functions always appear together. This procedure derives from the expression

$$b(x,y) \doteq (\text{const.})F^{-1}\left[J_1 \cdot J_2 \cdots J_n \cdots J_N\right]^{1/N}$$

F^{-1} = Inverse Fourier transform

$J_n(p,q)$ = Fourier transform of $j_n(x,y)$

$j_n(x,y)$ = n^{th} of N subsections of blurred image

The square-shaped j_n overlap each other halfway; upper right and lower left corners of diagonally adjacent members touch each other's corners.[3]

Given b(x,y), Weiner optimization theory suggests that the filter function

$$H(p,q) = \frac{|J(p,q)|^2 B^*(p,q)}{|J(p,q)|^2|B(p,q)|^2 + \lambda^2 N_o}$$

λ^2 = Arbitrary positive constant, N_o = Noise spectral density, assumed white

---

[3]Validating the b-approximation:

$$j_n(x,y) \doteq i_n(x,y) * b(x,y)$$

$i_n(x,y)$ = n^{th} subsection of ideal image

$$\sum_{n=1}^{N} \ln J_n(p,q) \doteq \sum_{n=1}^{N} \ln I_n(p,q) + N \ln B(p,q)$$

$\ln(p,q), B(p,q)$ = Fourier transforms of $i_n(x,y), b(x,y)$

$$\sum_{n=1}^{N} \ln I_n(p,q) \doteq N \langle \ln I_n \rangle_{\text{average}} \doteq \text{constant}$$

This permits an expression for B(p,q) in terms of the $J_n(p,q)$. Inverse transformation then gives the approximation for b(x,y) in the text.

will produce deblurring. As before, capitalized quantities represent Fourier transforms of their lower case counterparts. Constant λ^2 establishes the tradeoff between good deblurring on one hand and efficient noise rejection on the other. Physically, it governs filter bandwidth.

Haar implementations of b-identification and b-inversion are presently being studied. The b-identification process, which requires inverse Fourier transforms of products of Nth roots faces formidable difficulties. Other approaches may have to be considered. The b-inversion process, however, offers more opportunity for Haar innovation since

$$H \doteq \begin{cases} 1/B \quad \text{for} \quad |J|^2 >> N_o \\ \\ \dfrac{B^*}{\lambda^2 (N_o/|J|^2)} \quad \text{for} \quad |J|^2 << N_o \end{cases}$$

suggests a piecewise approach to implementation.

5.2.2.2.2 Experimental Procedure - Experimental tests on b-inversion can be conducted even while the overall procedure awaits further adaption to the Haar domain. These tests begin with an imperfect image j(x,y) whose blurring is due to a known b(x,y). Examples include a pinhole camera photograph whose b(x,y) follows from the numerical value of the hole diameter. Haar expansions of b(x,y) and j(x,y) can be combined in various ways, using the above piecewise approximation as a rough guide. Inverse Haar transformation then permits direct evaluation of the result.

One way of combining the two functions to achieve possible deblurring would take the Haar transform of b and average all coefficients of a given sequency r. Designating the average coefficient as a(r), one would multiply each Haar coefficient of j(x,y) by either 1/a(r) or k a(r); k = constant. The choice depends upon whether the

coefficient exceeds or falls below some present threshold, respectively. Different threshold settings and different values of k can be tried.

5.2.2.3 Depth of Field Blur - Since this difficulty nevertheless permits all various parts of the observed field to be brought into focus with different lens settings, a possible solution consists in recording Haar transforms of a given scene with several different lens settings. These settings should cover a range over which all parts of the scene come into focus. The variation of any particular Haar coefficient over the range can then be interpolated from the recorded samples, and the maximum magnitude evaluated. This maximum represents the in-focus value of the Haar term under consideration. Accordingly, the several Haar expansions can be replaced by one based on the interpolated maxima. The inverse transform should then yield an image simultaneously in focus at all points. In practical operation, the required multiple lens setting may be achievable via the same dither motion used in autofocus.

5.2.2.4 Jittered Images -

5.2.2.4.1 Concept - Given the Haar image expansion

$$i(x,y) = \sum_{rmpn} a(r,m,p,n)h(r,m,x)h(p,n,y)$$

$h(r,m,x)$ = one-dimensional Haar function of sequency r and offset m

$a(r,m,p,n)$ = Haar expansion coefficient

analysis[4] shows that sinusoidal jitter variations $\Delta x \sin wt$ change the above coefficients to time varying quantities:

$$a(r,m+2^r \Delta x \sin wt,n,p)$$

[4] Because $h(r,m,x) = 2^{r/2} h(o,o,x-m.2^{-r})$, x-directed jitter variations can be interpreted as equivalent variations in m.

Image jitter can therefore be corrected in the Haar domain by dithering the value of m to cancel this variation:

$$\text{Set } m = \hat{m} - \Delta m(t)$$

$$\hat{m} = \text{constant}$$

$$\Delta m(t) = 2^{r} \Delta x \sin wt$$

The resulting $a(r,\hat{m},p,n)$ can be inverse-transformed to create an unjittered image.

The above remarks have simplified matters by treating m as a continuous variable. Since m is in fact discrete, one approximate approach would replace $\Delta m(t)$ by the nearest integer. Other approaches based on interpolation between a-coefficients with successive m remain to be studied.

These remarks assume that the jitter is sinusoidal, and that the phase and amplitude can be detected. The sinusoidal assumption follows from the fact that underdamped gyros or marginally stable servos are often characterized by a single critical resonance. Phase can be determined from the periodic nature of the a-variation. Amplitude determination based on closed loop analogs is presently under study.

5.2.2.4.2 Experimental Approach - Experimental verification of this approach consists in jittering test patterns sinusoidally, using a variety of amplitudes and frequencies. The patterns might consist of vertical bars of various uniform widths. These widths can be correlated with the Haar functions that seem to react most sensitively to the jitter. For convenience, the jitter can be performed quasi-statically.

5.2.3 Image Enhancement

5.2.3.1 Objective - Image enhancement covers control over brightness, contrast, edge definition, and information content. As in autofocus, manual control is impractical. The eye-brain combination may furthermore fail to provide an adequate enhancement criterion, sacrificing information content for cosmetic appearance. Current plans therefore call for determining the Haar sensitivity to control brightness, contrast, edge definition, and information content for the enhancement concepts that follow.

5.2.3.2 Brightness Control -

5.2.3.2.1 Concept - Improper brightness level can lead to inefficient use of available gray shade levels in the display. Brightness corresponds to the coefficient of the Haar term

$$h(-1,1,x)h(-1,1,y) = h_{dc}$$

when the expansion includes the entire scene. When the expansion involves only a 16x16 pel block, however, the coefficient expresses the local tone. Under these conditions, brightness corresponds to the average of the local tone over all 16x16 pel blocks within the scene.

Automatic brightness control consists of regulating this coefficient.

One approach evaluates the average coefficient b_1, selects a desired brightness level b_2, and effectively adds b_2-b_1 to t_i, the h_{dc} coefficient of ith 16x16 pel block. Figure 5-5 outlines the process, using a linear analog of the two-dimension format.

This process destroys information contained in the brightness level. Should this prove significant, an attenuation element K within the AVG block will produce a brightness level of $b_2 + Kb_1$, K = 1-positive constant, which can possess a moderate response to scene[5] changes Δb_1.

5.2.3.2.2 Experimental Procedure - With different neutral density filters in front of the camera, measurements of t_1, t_2, t_3, ..., t'_1, t'_2, t'_3, ..., b_1 and b_2 can be made. The t_i should respond to filter changes, but the t'_i should not. If response time measurements are not considered important, the portion of the test setup between t_i and t'_i can be computer simulated.

[5] If K> (rms noise voltage)/Δb_1, brightness information will generally be preserved.

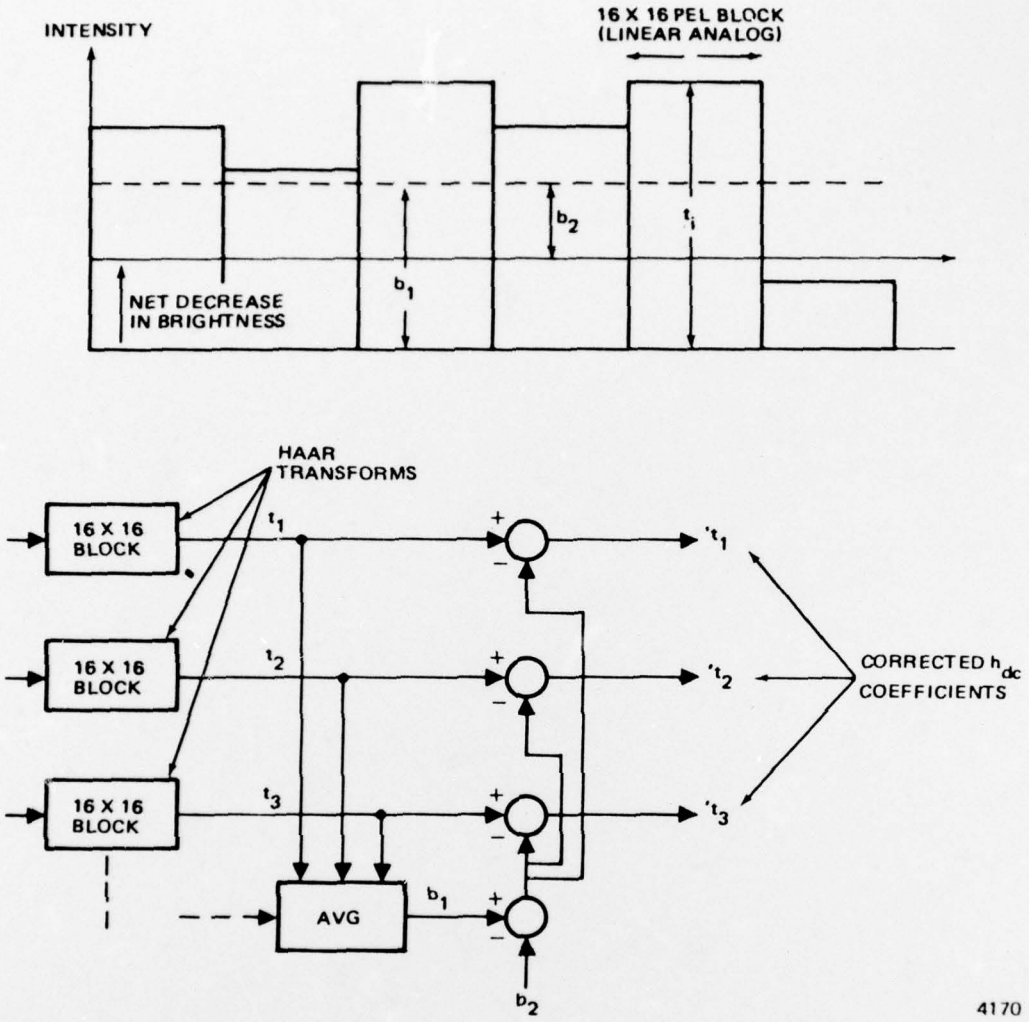

Figure 5-5. BRIGHTNESS CONTROL SCHEME

5.2.3.3 Contrast Control -

5.2.3.3.1 Concept - As in brightness control, improper contrast setting leads to inefficient use of available gray shade levels in the display. Contrast and activity represent distinct properties of a scene. The first refers to minimum and maximum gray shade levels while the second measures mean square intensity deviation. Contrast, furthermore, does not possess a straightforward expression in the Haar domain, while activity does. The two properties nevertheless possess a gross similarity, since they tend to increase and decrease with one another.

A reasonable solution concept might therefore consist of using Haar-derived activity as a measure of contrast. The inverse transform from the Haar domain to the reconstructed image would then use this measure as a means of contrast control. Activity can be conveniently expressed as the sum of squares of all Haar coefficients, excepting the h_{dc} term. The resulting quantity would be used for compensatory gain control in the inverse transform.

The prime counterexample to this approach is a scene which largely occupies only a few gray shades about the neutral level but which nevertheless contains one or two hotspots or coldspots. This scene would possess low activity and high contrast. Compensatory control would respond to the low activity by producing a high gain, driving hotspots and coldspots into saturation. Information penalties should be small, however, since pictorial details would not be lost.

5.2.3.3.2 Experimental Approach - Calibrated inputs may consist of different sample scenes representing varying degrees of contrast about a fixed brightness level. Alternatively, inputs can be achieved just by turning the contrast control knob on the recording camera. Variations in Haar transform coefficients in response to contrast changes, and the relative constancy of the h_{dc} term, can then be measured.

Off-line processing can provide the compensatory gain control. Contrast level in the final image can be measured by means of peak- and minimum-voltage detectors at the TV display.

5.2.3.4 Edge Definition -

5.2.3.4.1 Concept - Edge definition, or enhancement, can clarify the outline of potentially important shapes within the perceived image field. As such it is closely related to clutter suppression.

Within the Haar transform domain, edge and texture qualities tend to overlap. Texture often consists of fine edge-like details. These, however, lack the continuity quality of true edges, extending over only a few pels. Other textural aspects furthermore correspond to spots whose Haar properties remain distinct from edges. Thus, the overlap between edge and texture properties is only partial.

In view of these remarks, simple edge enhancement algorithms will include some texture features. Elimination of these features would require more refined algorithms of presently unknown complexity.[6]

One simple algorithm represents edges as the difference between focused and moderately defocused images. In the Haar domain, the defocused image cuts off all sequencies above relatively restricted limits. Otherwise, the transforms are essentially the same. Edge-seeking via differencing therefore subtracts the two transforms, leaving nonzero coefficients only in a band adjoining the high sequency borders. Enhancement amounts to adding this result to the transform of the original image. Equivalently, it simply amplifies the highest sequency Haar functions of the original image.

5.2.3.4.2 Experimental Approach - Verification follows from taking the Haar transform of superimposed photographic transparencies. One is a high-contrast positive, while the other is a lower-contrast, moderately blurred negative of the identical scene. The inherent subtraction emphasizes edges by suppressing nonedges. Results can be compared with a transform of the positive transparency alone.

5.2.3.5 Texture Definition - Solution concepts and experimental procedure follow from the preceding discussion of edge enhancement. To include spot-like contributions to texture, the band adjoining the high sequency borders must be broadened. It can, in fact, include all sequencies except h_{dc} for the 16x16 pel block under consideration.

5.2.3.6 Information Content -

5.2.3.6.1 Concept - Although maximum bandwidth is usually desired to utilize the maximum available system resolution, information content of a given scene can be degraded by choosing a pass band that is too high for the MTF of the imaging system. The excess bandwidth passes excess noise, thereby degrading the signal-to-noise ratio (SNR) and information content:

---

[6] One possible approach might consist of comparing in-focus and slightly defocused images, to see if the change suppresses texture while retaining major edge features. Another algorithm might measure edge length, rejecting those which fall below a specified limit. Definite recommendations, however, must await further study.

$$I(\text{bits}) = \frac{(\text{Image Area})}{(\text{Resolution Cell Size})} \log_2 (1+\text{SNR})$$

Insufficient bandwidth also degrades I by increasing resolution cell size.

Optimum filter theory reconciles these conflicting tendencies by choosing an algorithm which minimizes noise subject to a given transient error.[7]

5.2.3.6.2 Experimental Approach - In line with footnote 7 below, the noise floor of the Haar transform of a given image would be evaluated. This corresponds to the asymptotic level that squared coefficients appear to approach at the highest sequencies. For this purpose, the Haar transform should contain sequencies well beyond the highest ones present in the image.

The squared Haar spectrum will sink to selected multiples of this level at certain sequencies. Optimization of image information content then calls for using only that portion of the Haar domain that falls below these sequencies to reconstruct the image. Various multiples a^2 should be selected. Results will generally show that lower a^2 give crisper but noisier pictures.

5.2.4 Adaptive Signal Processing

Specific tasks under this heading include d-c restoration and dynamic range compression. D-c restoration covers distortions arising from a-c coupling of FLIR photodetectors to the electronics. Dynamic range compression maximizes utilization of the available number of gray levels in the display.

---

[7] Transient error is the mean square deviation between noise-free images before and after applying the algorithm. Noise refers to that part of the original image noise power spectrum N which the algorithm fails to block. In Fourier transform terminology, the algorithm corresponds to filter H and the original image to signal G. Variational calculus shows that $H = |G1^2/(|G1^2+a^2N)$ represents the desired filter. Different choices of Lagrange multiplier a^2 yield different tradeoffs between transient error and noise. Physically, a^2 corresponds to bandwidth. To a first order approximation this filter stipulates unit gain for all spectral regions exceeding an a^2 multiple of the noise. Regions below this level are completely blocked.

5.2.4.1 D-C Restoration -

5.2.4.1.1 Objectives - Lack of d-c restoration in the FLIR system creates three characteristic difficulties: Lost horizon, blacker-than-black and non-linear operation. Lost horizon might arise from two adjacent horizontally scanned lines, one above the horizon (bright) and the other below (dark). In passing through the a-c amplifier, the respectively high and low d-c pedestals will tend to decay to a common intermediate gray tone.[8] Cold bars limit the decay by effectively re-imposing initial conditions at the beginning of each successive scan.[9] Drift in cold bar bias level however can squeeze all available a-c borne picture information into a few display gray levels, leaving the others unused. Automatic bias adaption would therefore fill a cogent need.

5.2.4.1.2 Concept - The cold bar basically interjects negative rectangular pulses at points where one scan of a given line ends and a new one begins. These pulses convert a prolonged d-c pedestal extending over many scans into an a-c waveform. Short single-scan pedestals counterbalance the negative pulses to produce a long-term zero average in the new waveform. Pedestal shortening relaxes time constant requirements governing a-c amplifier low-frequency cutoff. This in turn reduces susceptibility to (1/f)-noise.

Incorrect pulse amplitudes however can force the pedestals to assume inappropriate settings, which utilize the available display gray levels inefficiently. Haar transform processing can relieve this difficulty. It intervenes beween sensor and display, and can adjust the capacity of one to the other. Specific corrective schemes will resemble Haar brightness control, discussed earlier. These schemes however cannot impose absolute control, which would negate all scene-brightness changes, since this may destroy important information. Moderated control can be achieved by proper feedback design within the Haar-domain portion of the processor.

---

[8] Negative step-signal changes from this incorrect gray tone (rather than the correct, brighter, value) plunge to voltage levels below absolute black; i.e., blacker than black. Positive steps would similarly create whiter than white. If there are too few voltage levels to accommodate the plunge, saturation sets in.

[9] Decay would only cause severe disability if continued over many scans.

The ability of the cold bar to minimize transient decay increases with scan speed.[10]

However, a small residual of the decay trend will always remain, tilting the bright pedestals downward (in time), and dark ones upward, toward the common median gray level. Should this prove objectionable, additional Haar corrective measures can be applied. These measures would recognize that within any sequency Haar functions with larger m suffer greater decay.[11] Haar coefficients for larger m can accordingly be amplified a little more to nullify the decay. Amplification can vary linearly with m, or can follow some simple polynomial law, depending upon the desired completeness of the nullification.

In conjunction with the preceding work on d-c restoration, the effects of scanning without a cold bar (or other form of vertical reference) will be investigated.

5.2.4.1.3 Experimental Procedure - Digitized images will be input to the IBM 370 computer and their scan lines will be subjected to various amounts of a-c coupling in order to simulate the initial conditions of the d-c restoration problem. Because of the one-dimensional nature of the problem, experimental verification requires observation of the pedestal height of only one scan line at a time. Feedback algorithms can moderate this height via the d-c Haar function. Preliminary study suggests that the feedback loop gain can be a relatively low bandwidth function with a moderately large amplitude level at dc. Transient-tilt correction will investigate similar algorithms operating on the higher sequency Haar functions.

5.2.4.2 Dynamic Range Compression -

5.2.4.2.1 Objective - Dynamic range compression attempts maximum utilization of the available display gray levels, since these are generally quite limited. It tends to amplify small contrast variations at the cost of moderating large ones. Usually, the tradeoff is highly advantageous both in terms of cosmetic appearance and information gain. The process proposed here is related to histogram equalization, but possesses several distinctive features which suit it to a Haar implementation. Haar implementation in turn raises the possibility of real-time operation.

---

[10] Scan speed cannot increase indefinitely, since the upper frequency cutoff limit of the photodetectors would ultimately be reached.

[11] This assumes unidirectional rather than racetrack scan. With slight modification, the above corrective procedure can accommodate racetrack scans as well.

5.2.4.2.2 Concept - Histogram equalization regulates the small signal gain at each amplitude in proportion to the number of pels in the scene which occupy that amplitude. Gain savings achieved in the low occupancy amplitudes can be passed on to the high occupancy amplitudes.[12]

One application would simply apply histogram equalization to the ensemble of h_{dc} from all the 16x16 pel blocks within the original scene. Picture tone would then undergo dynamic range equalization, but fine intensity variations within each block would remain unaffected. The possibility that these variations may also require dynamic range compression raises a potential difficulty. This difficulty can be addressed through a modified version of the general scheme: All Haar coefficients for a given sequency r would be amplified in proportion to the number of offset values m that are occupied. Occupancy, here, is the number of m whose coefficients exceed a preset threshold magnitude. Designating this number by M(r), the gain G(r) can be expressed as

$$G(r) = \frac{M(r)\cdot 2^{-r}}{\sum_{\text{all sequencies, } q} M(q)\cdot 2^{-q}}$$

Normalizing term 2^{-r} = maximum possible value of M(r); i.e., for full occupancy.

The ability of this approach to reproduce the desirable qualities of formal histogram equalization, and possibly to improve on them, is currently being analyzed. As in formal equalization, a derivative approach that treats one localized region at a time[13] will be considered.

5.2.4.2.3 Experimental Procedure - Experimental examination of the G(r) approach can proceed independently from the theoretical study of its capabilities. This examination can compute G(r) for each of a number of scenes and observe its effect

---

[12] Total variation in output gray level = $\int$ Small signal gain d Input gray level This integral cannot exceed an allowed upper bound. Since small signal gain must be a monotonically increasing function, lowered values of the integrand in certain intervals of the input gray level scale permit raised values in other regions without exceeding stated bounds.

[13] Termed "Local Area Histogram Equalization" or LAHE in the literature.

on the reconstituted image. In addition, any tendency of G(r) to assume a representative form applicable to a class of scenes (e.g., ground scenes) can be evaluated.

5.2.5 Data Compression

Data compression bears a certain resemblance to Dynamic Range Compression (DRC) but the goals are different. Here, the goal consists of maximizing information content for a limited bit capacity rather than the equally likely utilization of all bit levels (histogram equalization).

5.2.5.1 Objectives - Data compression explores the means for acquiring all necessary picture information with the minimum number of bits. This is advantageous where a data link is utilized to transmit FLIR images (in real time) to a remote terminal.

5.2.5.2 Concept - Three different approaches are being considered. One approach simply eliminates all Haar terms beyond a present sequency limit. The second eliminates all terms whose coefficients fall below a stated threshold, while the third approach applies thresholding to different sequency ranges.

The first approach is clearly the simplest, but probably the least efficient. Further insight may be gained from empirical evaluation, such as general rules for specifying the limit. Thresholding, as used in the second approach, should prove more effective. This approach tends to discriminate against low-SNR contributions to image data.

Such thresholding, however, can conceivably preserve many Haar components in one sequency range while destroying all components in another. It may then prove that sacrificing some components in the first range to provide bit capacity for representing a few components in the second range will be advantageous despite a net loss in SNR.

The third approach follows this reasoning. It subdivides the sequency range into low and high zones and thresholds each one. These zones in turn can be selected to characterize tone and edge qualities.

5.2.5.3 Experimental Procedure - The three approaches can be tried with a variety of scenes. Qualitative tradeoffs between simplicity and pictorial quality can be noted. Quantitatively, experimental measurements can determine a best setting for the present sequency limit in the first approach. These measurements will also determine whether this limit varies markedly from scene to scene, or if an all-purpose limit might be possible. Similar remarks apply to threshold settings in the second and third approaches.